3D PRINTING OF MICROWAVE AND MILLIMETER-WAVE FILTERS

Cristiano Tomassoni, Oscar Antonio Peverini, Giuseppe Venanzoni, Giuseppe Addamo, Fabio Paonessa, and Giuseppe Virone

A Brief Introduction to 3D Printing Technologies

3D printing, additive manufacturing (AM), digital manufacturing, and free-form fabrication are some of the synonymous expressions commonly used to identify the new class of processes through which objects are built by selectively adding material, usually layer by layer, instead of subtracting material, as in conventional machining techniques like chemical etching, laser-cutting, milling, and electro-erosion [ASTM01].

At first, 3D printing was applied to the rapid prototyping of new concepts and ideas, where plastic models were built to check the design before developing final products. In the last ten years, as the accuracy and the material properties improved, these technologies have started to be applied to build end-use components, largely because of several advantages [Wohlers01], among them

- Near net-shaped parts with complex shapes can be easily manufactured.
- Lightweight structures, like cellular or honeycomb structures, do not slow down the manufacturing process.
- Weight of objects is reduced, while saving material and energy.
- Design can be optimized for functionality.
- Lead time is optimized for small batch jobs.
- No tooling is needed.

At the same time, before end-use products that are fully complaints with the specifications of the relevant application domains can be achieved, some technological barriers still need to be overcome, such as:

- High costs of machines and raw materials.
- Slow deposition rates, since parts are manufactured layer-by-layer with a layer thickness typically in the range of 0.025-0.250 mm.
- The use of metal alloys that are not specifically designed for AM.
- Unprocessed material and supports have to be removed after printing.
- Post-processing treatments, such as synthetization, stress-relieving, and shot-peening, are required.
- AM technologies change rapidly, so it may be difficult to define a business model.
- Dimensional accuracy and repeatability are lower than with conventional machining techniques.

A few examples of markets that are currently taking advantage of the availability of these new processes are [Hao01], [Manfredi01], [Guo01]:

- Digital dentistry and bio-medicine, since the design flexibility provided by 3D printing eases the customization of orthodontic implants and prostheses.
- The aerospace industry, where AM allows for the manufacturing of new layouts of structural brackets based on organic shapes that are optimized in terms of stiffness and lightness.
- The automotive industry that can now rely on complex shapes implemented in monolithic parts without the need for welding.

Additive manufacturing of microwave and millimeter-wave components (including filters) has been investigated since approximately 2014, as seems clear from publication trends in this topic in the IEEE Xplore digital library (see the pie chart of Fig. A01).

Based on our analysis on these papers, the AM processes most commonly investigated for radio-frequency (RF) applications are material extrusion, material jetting, vat photo-polymerization, and powder bed fusion.

Getting inside the Additive Manufacturing Workflow

Despite the differences among the various AM technologies, there are eight steps that all 3D printing processes must go through in order to achieve a final product that is ready for application; the steps are shown in the generic workflow in Fig. A02 [Gibson01]. These steps are:

CAD. The 3D Computer-Aided-Design (CAD) model is developed via a 3D design program or a reverse engineering process.

Stereolithography file (STL) conversion. The CAD model is converted into an STL format describing the object surface as a mesh of triangles. The parameters of the STL triangularization determine the shape approximation error.

Transfer to the AM machine. The part is positioned in the building chamber so as to minimize the stair-case approximation, the risk of warping and collapse, and the use of supporting structures.

Setup. The process parameters of the AM machine are set depending on the specific material, layer thickness, and building speed.

Build. The manufacturing process is completely automated and usually no supervision is needed.

Remove. Removing supporting structures can be a manual task that requires careful attention and can damage the components.

Post-process. The processes applied at this step depend on the final application of the part. Thermal treatment and surface finishing operations, like sandpapering, shot-peening or polishing, are common

processes for every technology. Other processes can be surface-coating and infiltration to increase the strength of the parts.

Application. The properties of AM components can be different from those of the same components built with standard manufacturing. For this reason, depending on the intended application, ad-hoc standardization and qualification procedures have to be defined.

Material Extrusion at a Glance

In the material extrusion process (Fig. A03), a filament of polymeric material is heated and, then, dispensed through a nozzle. The latter is moved by a robot arm that retraces the desired shape of the part. The material to be printed is kept in a molten state inside a liquefier chamber at the lowest temperature possible, since some polymers degrade at high temperature. Sometimes, two nozzles are used: one deposits the building thermoplastic material, while the other prints the supporting structures. The diameter of the nozzle determines the size of the extruded filament and the minimum feature size that can be printed. The larger the nozzle diameter, the faster the process, but with lower precision. Bonding between consecutive layers can be achieved by residual heat energy or by solvents and wetting agents contained in the extruded filament. Materials typically used in material extrusion are filaments of thermoplastics coiled onto a spool. A large number of thermoplastic materials are available for these processes [Calignano01], including:

- Acrylonitrile Butadiene Styrene (ABS): a common thermoplastic material used in injection molding processes with good properties in terms of hardness, strength, and heat resistance. Different ABS-like materials have been developed with specific properties and colors.
- PolyLactic Acid (PLA): a biodegradable plastic obtained from renewable resources, such as corn or sugar cane. Although the mechanical properties of PLA are inferior to those of ABS,

PLA is one of the materials most used in low-cost printers because of its environmental sustainability. Different colors and types of PLA are also available.

- Nylon: a generic term for a category of polyamide materials. The nylon material most commonly used in fused filament fabrication (FFF) is Nylon 12 (PA12), because it exhibits good strength and a low friction coefficient.
- PolyEtherEtherKetone (PEEK): a high-performance organic thermoplastic material with high heat and chemical resistance and good strength.

From Inkjet Printing to Material Jetting

Material jetting is based on the deposition of droplets of material through moveable printer heads (Fig. A04), thus making this process category quite similar to inkjet printing. Multi-nozzle printer heads can be used to increase speed and to create multi-material parts [Wohlers01]. The printed traces are then cured using a UV lamp that follows the heads. Droplet formation is one of the steps that most influence printing quality. Available technologies for droplet formation are continuous stream (CS) and drop-on-demand (DOD). In CS systems, droplets are produced at constant intervals through steady pressure applied to the fluid reservoir. In DOD systems, droplets are produced only when a pressure pulse is applied to the nozzle. This pressure is created by an actuator that, in most cases, is thermal or piezoelectric. In thermal systems, a resistor heats the liquid in a reservoir until a bubble expands and a droplet is ejected from the nozzle. In piezoelectric systems, the droplet is ejected because the deformation of a piezoelectric element reduces the volume in the reservoir. Photopolymers and wax-like materials with specific viscosity properties are typically used. To lower viscosity, solvents can be added to the printable materials.

Powder Bed Fusion Technologies

In powder bed fusion processes, a layer of powder is spread over a platform, using a roller or a blade (Fig. A05). Then, a laser or an electron beam is used to selectively fuse the powder particles. The platform is lowered, and the process is repeated until the part is built. At the end of the manufacturing job, the parts are removed and cleaned of unprocessed powder. This technology was originally developed for plastic materials and, then, extended to metal and ceramic powders. The fusion mechanisms most used are liquid-phase sintering and full melting. In liquid-phase sintering, a portion of powder particles becomes molten, while the other part remains solid. The molten part works as a glue that binds the solid part. In full melting, the powder is melted to a depth that is greater than the layer thickness, so that the previous layer is re-melted, thus leading to high density and well bonded parts. The most commonly used powder-bed-fusion processes are:

- Selective Laser Sintering (SLS). SLS is a liquid-phase sintering process mainly applied to build parts made of polymers or composites using a CO_2 laser. Powders are pre-heated before being spread over the build area and, then, infrared heaters are used to maintain a temperature just below the melting point and the glass transition temperature of the material. Parts are built inside a chamber filled with nitrogen gas, in order to minimize oxidation and degradation of the powders.
- Selective Laser Melting (SLM). SLM is a full melting process developed for metal and ceramic powders. The main difference with respect to SLS are the lasers used. Indeed, the SLM lasers have to provide a wavelength compatible with the absorptivity of the metal/ceramic powders and a power level sufficient to heat the powder above the melting point. Due to the high thermal

gradients arising during the manufacturing, a stress-relieving post-processing is carried out inside an oven at the end of the job. Mechanical properties of SLM parts are similar or even better to those obtained by conventional machining.

- Electron Beam Melting (EBM). EBM is a process developed for metal and ceramic powders based on the use of a high-energy electron beam inside a vacuum chamber. The high energy of the electron beam heats the powder to a higher temperature than a laser can achieve. As a consequence, the temperature of the powder bed in EBM is higher than it is in SLM. The result is a part with less residual stresses than SLM and a microstructure completely different compared with that of an SLM part. EBM is faster than SLM, but the surface finishing is worse [Wohlers01].

Vat Photopolymerization

Vat photopolymerization systems consist of a vat full of liquid resin, a platform that can be moved up and down in the vat, and a radiation source, usually a laser or a UV light, that activates the selective polymerization of a photosensitive liquid resin (Figure A06). After building, the parts are placed into an UV oven to complete the curing. The main difference among available vat photopolymerization systems is the scanning scheme. Stereolithography (SLA) is a widespread vat-photopolymerization process that implements the vector scan approach (Figure A07(a)), where a laser beam scans the surface according the desired trace to be printed on the layer [Guo01]. Direct light processing (DLP) is based, instead, on mask projection, where a large beam irradiates the entire layer at one time (Figure A07(b)), thus resulting in a faster approach. Modern DLP systems use digital micromirror devices as dynamic masks and UV lamps or visible light as their radiation source. The main advantage of vat polymerization with respect to other AM technologies is its good surface finishing, since average surface roughness Ra can

be on the order of a few μm. A wide range of materials is available for vat photopolymerization, including ABS-like and ceramic-like materials [Hinczewski01].

Direct Metal Printing of Waveguide Filters through Selective Laser Melting

In recent years, the powder-bed-fusion technology commonly investigated for microwave and millimeter-wave components has been selective laser melting. Indeed, this technology allows for the direct manufacturing of metal parts with good mechanical and thermal properties, such as stiffness, thermal conductivity, and thermal expansion coefficient. Different metal powders are available for this process, including stainless steel, nickel-based alloys, aluminum alloys (e.g., AlSi10Mg), and titanium alloys (e.g., Ti6Al4V). Depending on the specific metal powder used, surface coating for achieving high electrical conductivity may be unnecessary. This aspect enables the manufacturing of complex monolithic components, thus minimizing the number of mechanical parts used in radio-frequency (RF) systems. This translates, in turn, into a minimization of mass, envelope, interface flanges, and test procedures [Booth01], [Peverini01]. For these reasons, SLM has already been investigated for the manufacturing of several waveguide components, such as feed-horns [Addamo01], septum polarizers, couplers [Chio01], meander waveguides, and orthomode transducers [Kilian01], [Addamo02]. Manufacturing of monolithic complex RF systems, such as slot antenna arrays [Chio01] and Butler matrices [Crestvolant01], has already been demonstrated.

The first pioneering work on the application of selective laser melting to the manufacturing of waveguide filters was published in 2009 by Lorente *et al.* [Lorente01]. In this work, the SLM process was used to manufacture 5th-order Chebyshev band-pass filters working in the Ku-band (center frequency = 11 GHz, bandwidth = 100 MHz). The filters, consisting of rectangular cavities coupled via inductive E-plane irises (shown in Fig. B01(a)), were manufactured in both aluminum (AlSi10Mg) and

titanium (Grade 2) alloys. The dimensional accuracy of the process was previously estimated from a filter sample that was cut and measured inside. The measurements indicated that the dimensional standard deviation was in the range of 0.05 mm to 0.15 mm, thus making the use of tuning screws necessary to recover the targeted specifications. Thanks to the higher design flexibility provided by SLM, shaping of cavities and irises, as shown in Fig. B01(b), was also investigated for the purpose of compensating for the effects of the high surface roughness provided by this process. Indeed, the arithmetical mean height (Ra) surface roughness was measured to be approximately 15 μm for the Al samples and 9 μm for the Ti samples. These values are about one order of magnitude higher than those commonly achievable by milling. This implies that the values of the equivalent surface electrical resistivity, accounting for both the bulk material electrical resistivity and the surface roughness, were rather high, that is, approximately 6 μΩcm for Al and 50 μΩcm for Ti, respectively. These values led to a degradation of the quality (Q) factor of the filters, as summarized in Table B01, where the measured Q-factors of the prototypes are compared to the reference value of the standard layout filter manufactured in aluminum (Q factor ~ 4000). In order to improve the Q-factor, silver plating of the aluminum filters and chemical polishing of the titanium prototypes were carried out. From the measured results, it is evident that silver plating is mandatory for Ti-based filters, because the equivalent surface electrical resistivity is mainly driven by the bulk resistivity of the titanium material. At the same time, due to the low electrical resistivity (on the order of 1.6 μΩcm) silver coating can be applied to achieve Al-based SLM filters with very high quality factors.

The main outcome from [Lorente01] is the evidence that shaping of cavities and coupling structures can compensate for the increased surface roughness in SLM filters. This concept was later exploited by Booth *et al.* in [Booth02], where the influence of the surface roughness was counterbalanced by implementing new complex geometries of cavities and irises in monolithic in-line filters working in the

Ku-band (passband = 14 - 14.25 GHz). Specifically, Booth *et al.* studied different cavity shapes in view of increasing the Q factor and the higher-order resonance frequencies. The latter parameter is a key driver for achieving broad spurious-free ranges, that is, large stopbands with high rejection with respect to higher-order modes. In [Booth02], it was shown that an ellipsoid cavity compares favorably with respect to a homogeneous rectangular-waveguide cavity in terms of Q-factor and second eigenmode resonance. However, this geometry calls for intersection of adjacent cavities in order to implement the required coupling levels, thus leading to a detrimental impact on the overall performance of the filters. Cavity intersection can be avoided by using super-ellipsoid geometries that are defined by

$$\left(\left|\frac{x}{A}\right|^r + \left|\frac{y}{B}\right|^r\right)^{r/t} + \left|\frac{z}{C}\right|^t = 0,$$

where A, B, and C are the scaling factors along the three axes and the parameters r and t determine the flatness of the cavity. Further improvements (by approximately 13% and 27% for the quality factor and rejection band, respectively) with respect to a cuboid cavity were achieved by applying a depression to the center of the super-ellipsoid cavity, where the surface currents of the fundamental eigenmode are minimal. Figure B02(a) shows the overall structure of a 5th-order filter designed as a drop-in replacement for a standard waveguide filter in a satellite payload. The shaped filter manufactured through SLM in the proprietary Scalmalloy powder and then silver plated exhibits measured performance within the specifications (e.g., insertion loss lower than 0.2 dB and return loss higher than 20 dB), while being a monolithic component with a weight less than 60 g. Figure B02(b) shows an internal view of the manufactured filter taken by computed tomography scan, which was carried out in order to detect any defect or contamination. The flying model of the filter successfully passed all the space qualification tests (including vibration/thermal cycling and mechanical/thermal shocks), thus demonstrating that selective laser melting is a suitable manufacturing technology for RF filters intended for deployment in space. Later, in [Booth03], Booth *et al.* applied the super-ellipsoid cavity design to

more complex Ku/K-band filters with higher rejection levels and wider spurious-free ranges, thus showing the potential benefits of the free-form capability of the SLM process. This capability was also exploited by Sattler *et al.* in [Sattler01] for the development of a X-band 4th-order stepped impedance filter intended to be manufactured in a single mechanical part. To this end, the well-known mushroom-shaped resonators were modified in lollipop-shaped resonators that were inserted in a waveguide channel with an ellipsoid cross-section (Figure B03(a)). In this way, all the inner surfaces of the filter were self-supporting; that is, no additional mechanical structures were required to support the inner surfaces during printing of the filter along the vertical axis (i.e., the direction of the mushroom-shaped resonators). Although the filter was designed for monolithic manufacturing, it was printed in two shells (Figure B03(b)) so as to allow for investigation of the inner surface accuracy and to simplify both the silver-plating process and the mounting of the input coaxial connectors. Figure B03(c) shows a comparison between the predicted and measured scattering coefficients of the filter that was printed in stainless steel in order to achieve a high dimensional accuracy. Indeed, a general rule in machining is "the higher the material strength, the better the dimensional accuracy." However, the SLM process is a high-energy process, where a high-power laser (on the order of hundreds of watts) actually melts a bed of metal powders. As a consequence, during SLM manufacturing high thermal stresses arise inside the parts that depend on the material used (the higher the strength, the higher the melting point) and can lead to deformations. To minimize the latter, the parts still attached to the building platform undergo a stress-relieving process in an oven at high temperature (up to 700 ^{O}C for titanium parts). A comparative study among Ku/Ka-band filters printed in AlSi10Mg aluminum alloy, Ti6Al4V titanium alloy, and maraging steel is reported in [Peverini02]. Figure B04(a) shows the samples printed in different metal alloys through SLM along with a copper-plated prototype printed through SLA in an ABS-like resin. The filter geometry is based on a composited step-stub filter layout [Peverini03] that was previously proved in

[Peverini04] to be more suitable for 3D printing than other geometries, such as iris filters. The measured in-band reflection and out-of-band transmission coefficients are compared with the simulations in Figure B04(b) and Figure B04(c). It is worth noting that the titanium sample exhibited the higher reflection coefficient, notwithstanding its high material strength that should had led to higher dimensional accuracy compared to aluminum. The reason for this lack of accuracy was due to the high thermal stresses in the titanium parts, as neither the electromagnetic nor mechanical designs were oriented to aid SLM printing. In order to recover the expected accuracy for titanium parts, the RF design was modified as discussed in [Peverini04] by tilting the stubs downwards so that the filter could be manufactured by aligning the longitudinal propagation axis with the vertical building direction. In this alignment, the accuracy of the waveguide cross-section in the *x*-*y* plane depends on the beam-spot size and material shrinkage, while the profile along the waveguide propagation *z*-axis is only affected by the stair-case discretization of the profile due to the layer thickness (typically, 30 μm). In order to compensate for the systematic errors occurring in the *x*-*y* plane, fine tuning of the system parameters (*i.e.*, beam offset and scanning options [Manfredi01], [Calignano02]) was previously carried out by manufacturing different straight waveguide lines. The tuning of the process parameters was based on a comparison between the theoretical and measured values of the phase delay introduced by the lines. Additionally, the external profile of the filter was re-designed as shown in Figure B05(a) so as to maximize the heat transfer, giving rise to smaller thermal gradients during the manufacturing. As a result, the corresponding measured reflection and transmission coefficients agreed very well with the simulations for all the filter prototypes (Figure B05(b)(c)), and especially for the titanium sample, thus confirming the importance of tailoring the filter design to the SLM process. The corresponding dimensional accuracy was estimated to be in the range of 40-70 μm, while the surface roughness Ra was reduced to approximately 5 μm thanks to shot peening of the internal channels (i.e., abrasive glass/zirconia microspheres of 0.1 mm diameter

were pumped through the waveguide channels). The AM-oriented design based on the rotation/tilting of the internal discontinuities was also applied in [Booth04] in order to develop an 11th-order filter aimed at very high throughput satellites (VHTS) or constellations of small satellites. In this case, dimples were inserted at the center of the cavities to improve rejection and spurious-wide range.

Although the dimensional accuracy and resolution of the SLM process make this process more suitable for the manufacturing of RF filters working below 20-30 GHz, Zhang *et al.* presented in [Zhang01] two high-order Chebyshev filters working in the passbands [71, 76] GHz and [81, 86] GHz. The filters were based on the in-line arrangement of 15 and 11 cavities in a WR12 rectangular waveguide coupled by H-plane irises. The two prototypes were manufactured in CuSn15 alloy powder with a dimensional accuracy of 2-3 % and a surface roughness Ra of approximately 6 μm. These manufacturing properties resulted in a degradation of the frequency responses, above all in terms of passband frequency shift and insertion loss (on the order of 2-3 dB).

A possible way to extend the applicability of the SLM process to the manufacturing of filters working at high frequency bands is to adopt micro SLM systems. These systems are similar to standard SLM systems, but they make use of powders with smaller particle sizes. This translates into smaller beam-spot diameter, laser power, and layer thickness, thus increasing the accuracy, resolution, and surface finishing. A comparison of typical values for some of the main parameters of the SLM and micro SLM processes is reported in Table B02. In [Salek01], Salek *et al.* applied the micro SLM process to the manufacturing of two W-band 5th-order pass-band filters based on the in-line arrangement of WR10 waveguide cavities coupled via H-plane irises. The two prototypes were built in stainless steel, with one coated with copper. Figures B06(a)-(b) show the prototype as built, still attached to the building platform, and after copper plating, respectively. Thanks to the higher accuracy and surface finishing provided by the micro SLM process, the measured scattering coefficients compared well with the

predicted data, as reported in Figs. B06(c)-(d). Remarkably, the filter exhibited an in-band insertion loss of approximately 1 dB, corresponding to an equivalent surface electrical resistivity of 6.7 μΩcm. This rather low resistivity value was achieved thanks to a measured surface roughness of approximately 2 μm. Another promising technology for manufacturing high-frequency filters is the 3D screen printing process presented in [Dressler01], the application of which for RF components is currently under evaluation.

The state-of-the-art reported in this Section and summarized in Table B03 shows that selective laser melting can represent a viable solution for the monolithic manufacturing of waveguide filters working at high frequency bands, although some technological aspects have to be carefully considered, such as thermal stresses arising during the manufacturing and the staircase effect induced by the layer thickness. Additionally, the SLM process provides the unique capability of free-form fabrication of direct metal parts that can be exploited in order to miniaturize waveguide sub-systems that include several RF functionalities, among which are filters. An example of integration of three distinct RF functionalities in a single miniaturized part is reported in [Peverini05]. This paper considers a waveguide sub-assembly commonly implemented in antenna-feed systems, consisting of the cascade of a 90-degree H-plane bend, a Ku/K-band lowpass filter, and a 90-degree twist. Thanks to the free-form capability of the SLM process, the 9th-order filter, which is based on the topology presented in [Peverini03], is mapped into an H-plane bend with constant radius. Then, the geometry is uniformly twisted, yielding to the CAD model shown in Fig. B07(a). Three prototypes with different bend radii were manufactured via SLM in aluminum. Figure B07(b) shows a comparison between the measured and predicted scattering coefficients of the shorter prototype. Along with a very good RF performance (i.e., return loss higher than 22 dB, out-of-band rejection higher than 60 dB, and insertion loss lower than 0.15 dB), this component merges the bending and twisting functionalities in the filter structure without any additional

mass, volume, or interface demands. This aspect is of the utmost importance in several application domains, among which are satellite communication and automotive radar.

Development of Plastic Microwave Filters

As discussed above, there are several plastic deposition techniques that can be used to fabricate microwave components and in particular microwave filters. They are the material extrusion process, commonly known as fused deposition modeling (FDM), photopolymerization of a liquid resin, and material jetting, also known as PoliJet.

All of these techniques have been investigated in recent years, exposing their strengths and weaknesses. The papers in the literature can be divided into two classes. The topic of the papers belonging to the first class is the study of the feasibility of standard components built using 3D printing. This study is important in order to verify the possibility of fast and low-cost prototyping of components by additive manufacturing (AM). In this group there are also papers that propose methods to metallize the devices. The topic of the second class of papers is the study of new filter configurations that take full advantage of AM flexibility. In this case, these components can be easily built by 3D printing, but they are difficult to fabricate with traditional subtractive techniques.

Studies on Plastic Additive Manufacturing Technologies for Filters

Historically, the first attempts to use plastic 3D-printing concern the study of the feasibility of the different technologies to fabricate microwave components and the analysis of the results. The available literature can be classified according to technology. For FDM technology, one of the first attempts was presented in [Montejio01]. The authors fabricated a corrugated low-pass filter, a high-pass filter, and an inductive iris band pass filter. Fig. P01 shows the internal parts (air) and the external parts of the filters. In order to metallize the internal surfaces, all devices were split into two halves and the flanges were fabricated separately and then attached to the main bodies. In [Delhote01] the authors assessed the

technology by building two band-pass filters, a four-pole inductive iris filter and a two-pole with inductive posts (i.e., an E-plane filter), and a helical resonator used to test the dielectric constant of materials. In both articles, there is a slight frequency shift and return loss deterioration in the experimental responses compared to simulated ones. This means that the dimensional accuracy is not enough to avoid tuning elements, especially for narrow band filters. However, these papers show that polymer-based AM machines, such as cheap FDM printers, can be successfully used in university laboratories for rapid prototyping of RF components aimed at educational activities and for low-cost manufacturing of measurement equipment (such as waveguide jigs used in network analyzers setups). In [Jankovic01] other cavity filtering devices, working in the Ka band and made through FDM, were presented. Results, in terms of accuracy and frequency shift, are comparable with other works. In [Massoni01] a 3D printer was used to manufacture the waveguide enclosure of a high permittivity dielectric resonator. In this case, frequency accuracy and losses of the measured single pole filter mostly depended on the dielectric resonator.

In [Tomassoni01], [Tomassoni02], and [Tomassoni03] the possibility of using the infill percentage for local control of the dielectric constant and loss tangent of the printed material has been demonstrated through the additive manufacturing of a substrate integrated waveguide (SIW) (Fig. P02). To this end, two different substrates with different infill percentages (40% and 100%) were printed and used to build two SIW filters with the same filtering response.

FDM printers are less expensive than SLA or PoliJet printers. The filament is also very cheap, and PLA is eco-friendly. However, since the nozzle diameter is usually 0.25-0.4 mm and the layer thickness is in the range of 0.1-0.25 mm, mechanical accuracy is not very high. The surface roughness is also quite high, meaning that this technology is not very attractive for the fabrication of microwave components.

Another interesting technology is photopolymerization and, in particular, stereolithography (SLA or SL). Earlier works are [Chappell01], [Chappell02], [Chappell03] and [Chappell04], in which tests of simple waveguide cavities and filters were completed. The first example is a single cavity working in the Ku band, where the authors split the cavity without perturbing its current flow. Other tests concern horizontally and vertically shaped multi-cavity filters. The most complex device is the four-port waveguide filter shown in Fig. P03. The authors obtained quite good results, with a frequency shift of the response around 0.15% and quality factors for all prototypes in the range of 3000-3500. The experimental return loss is lower than the simulated one, but this difference is comparable with other fabrication processes. In [Tomassoni03] and [Tomassoni04] a single cavity and a three-pole waveguide filter working in the X band were presented. The cavities were shaped to make the metallization process easier. In this case, the frequency shift is around 0.15% and the measured quality factor is 3700.

Other tests have been carried out at higher frequencies. For example, in [Dauria01] a six-cavity filter with inductive irises working in the W band was presented. The experimental response is shifted at higher frequencies. The authors state that the problem is a metallization thicker than predicted that reduced the length of the cavities. Another example of a fifth-order waveguide filter operating in the W band is shown in [Shang01]. The filter was fabricated as a single piece with many apertures for the metallization of internal surfaces (Fig. P05). Considering that the prototype does not use any tuning elements, the experimental results show very good agreement with simulations, with only a small shift toward lower frequencies of the passband.

The results obtained with SLA are very good, thanks to the higher accuracy of this technology compared to FDM. In fact, the usual laser spot diameter is 50-100 μm and the layer thickness is 25 μm to 200 μm, depending on the printer. The roughness is also lower with respect to FDM, as it is on the order of a few

microns. Considering its good trade-off between cost and mechanical accuracy, this technology is one of the most used and most promising for the fabrication of 3D printed components.

Some attempts have also been made using PoliJet technology. For example, in [Cai01] basic single and multi-cavity waveguide filters were fabricated. PoliJet's accuracy is higher than that of either FDM or SLA. In particular, both the lateral and vertical resolutions are around 15 μm, with a roughness of the surfaces that varies from 0.5 μm for horizontal surfaces to 3 μm for vertical surfaces. The latter figure is mainly due to the layer-by-layer deposition. PoliJet technology has also been used to build planar filters, by printing the substrate as in [Park01]. However, the high loss tangent of the resin gives quite lossy devices. A very recent work shows an application of PoliJet printing in the Ka band [Lucyszyn01]. In this case a gap waveguide (i.e., with non-continuous side walls) four-pole filter was fabricated and tested (Fig. P06). As can be seen, there is capacitive cross-coupling between cavities 1 and 4 that creates the two transmission zeros. This experiment shows that the 3D printing of such devices is feasible, and the experimental results are in good agreement with the theoretical results. The accuracy of PoliJet technology is higher than FDM and SLA. In fact, the typical lateral resolution and layer thickness are in the range of 15-30 μm. The measured roughness is around 0.5 μm.

In [Craton01], an aerosol jet printing (AJP) process was used to build a planar filter. This technique is relatively recent and consists of the jetting of a polyamide resin that only requires the post-processing step of high temperature curing. This step is also called imidization. The advantage of this technique is that the same printer can be used to fabricate both the dielectric and the conductive layers.

Since all the devices described above are made of plastic, they have to be metallized in order to realize conductive walls. Some techniques have been proposed; they are summarized in the following.

- Silver painting ([Montejo01], [Delhote01], [Jankovic01]). The device is metallized by painting with a silver ink. More than one layer can be applied; after that the previous layers are dried. This is the simplest metallization and the final conductivity of the surfaces is rather low, in the range of 10^5-10^6 S/m, thus the losses are higher than standard metal components.
- Silver painting + electrolytic copper ([Chappell01], [Chappell03], [Tomassoni04]). This method, fully described in [Tomassoni05], applies a double step process to metallized components. The first step is silver painting of the surfaces. This layer acts as an activation layer for the subsequent electrolytic copper plating, as electrolytic processes can be done only on conductive surfaces. The thickness of the copper layer can be up to several tenths of microns, depending on the duration of the deposition, and the dimensions of the device have to be adjusted in order to compensate for the thickness of this layer. With this method, a conductivity very close to that of pure copper and a roughness below 1μm can be obtained. As a consequence, the measured losses are usually comparable to the losses of traditional metal components. This process is also easy to implement and very low cost. As reported in [Tomassoni05], the metallization has a good adhesion to the plastic and the device is resistant against peeling.
- Electro-less copper deposition. This is a more complicated and expensive process, as it needs some activation before copper deposition. This process has been used with success to metallize components on internal surfaces, without the need to divide them into two or more parts, as shown in the work presented in the next section.

The copper can also be plated with a 100nm thick gold layer (as in [Shang01]) in order to protect the device from oxidation.

Innovative Filter Design using Additive Manufacturing on Plastic and Ceramics

Building upon early studies that showed the feasibility of 3D printed microwave devices, innovative microwave filter designs have been proposed that take advantage of the flexibility of AM technologies.

The first example concerns spherical resonator filters [Shang02], [Guo02], [Shang03]. Spherical resonator filters can be easily built using additive manufacturing, yet they are relatively complex to build with traditional subtractive manufacturing. In [Shang02], a single-mode cavity filter operating in the X-band was designed (Fig. P07). It uses a fundamental TM_{101} mode that exhibits a high quality factor. In [Guo02], [Shang03] a dual-mode cavity filter is proposed (Fig. P08). In this case the filter is fabricated as a single piece with apertures on the external walls to facilitate metallization of the internal surfaces by electrolytic copper deposition. The apertures are strategically placed where the currents are not perturbed. The experimental results are quite good, with a slightly higher insertion loss in the pass-band (0.3 dB measured vs. 0.1 dB simulated). The filter was tuned using small wires inserted inside the apertures in the lateral walls of the device. In [Wang01] a four-pole spherical cavity band-pass filter similar to that proposed in [Shang02] was built as a single piece and then metallized using an electroless nickel/copper plating. The experimental losses were higher with respect to the simulations.

A thorough discussion of hemispherical resonators is presented in [Yuan01]. The authors analyze many aspects of this approach, proposing different cavity arrangements in order to improve the out-of-band attenuation. Moreover, they analyze the coupling apertures among resonators. The prototypes were fabricated as single blocks and metallized using electroless copper deposition and silver plating. Experimental results are very good compared to the simulations.

Helical resonator filters are another type of filter that can take advantage of additive manufacturing [Shang04]. Helical resonators are useful at very low frequencies (usually VHF and UHF bands) and,

traditionally, are made by winding a wire by hand. 3D printing can automate the production while improving accuracy. In this article the authors propose a half-wavelength helix with variable width (Fig. P09). The shape of the helix is used to increase the filter bandwidth.

In [Delhote02] an innovative tunable E-plane filter, fabricated using FDM technology and operating at around 5.7 GHz, is proposed (Fig. P10). In this structure, the filter is composed of a waveguide, divided into two halves, and a sort of spiral ribbon that can rotate. Part of the spiral ribbon is inside the waveguide, and, with its rotation, the band of the filter can be shifted. The experimental results show the validity of the principle.

Another filter geometry that can take full advantage of additive manufacturing is the combline layout. Usually, a combline filter is made of several parts such as a housing, a cover, and a number of internal posts, one for each cavity, that are attached inside the housing. With AM, only two parts are needed, a main body that contains the resonators and a cover. The resonators can also be loaded with capacitive discs, thus resulting in the so-called “mushroom” shape, in order to reduce the length of the posts and improve the out-of-band attenuation. In [Tomassoni06] and [Tomassoni07] a basic doublet capable of responses with two poles and two transmission zeros, is presented. The coupling between the two resonators is achieved by a conductive rod attached to the mushroom stems. In [Tomassoni08] the basic structure was extended by cascading two basic doublets (Fig. P11), demonstrating the possibility of building higher order filters. As can be seen, with this structure it is simple to place a couple of transmission zeros above the pass band of the filter.

Another approach using mushroom-shaped resonators is presented in [Venanzoni01]. In this case, inductive and capacitive coupling between two resonators is achieved by a rod connecting the stems and by reducing the distance between the two “caps”, respectively (Fig. P12). The resulting coupling

generates a transmission zero. This zero can be placed above or below the band of the filter depending on the magnitude of the electric and magnetic couplings. The scattering parameters shown in Fig. P12b show that the structure is able to generate the two transmission zeros. There is a small shift of the band of the filter toward higher frequencies.

In [Tomassoni09] and [Tomassoni10] a very compact filtering structure is presented. The filter consists of a single septum with one or more apertures, and two small resonant posts (Fig. P13). A very precise positioning of the transmission zeros is possible in this filter by properly selecting the shape and dimension of the apertures and posts. This structure can be used to add a mild filtering behavior in existing microwave systems. Indeed, if the filter is inserted between the junction of two waveguides of an existing system, the system dimension increases only by the septum thickness (0.5 mm).

A filtering structure with high shaping flexibility is presented in [Venanzoni02]. In this case, there is a coaxial line that is attached to the main body with supports. The portions of the lines in the free air act as resonators, whereas the supports are the coupling elements (Fig. P14). The desired filter response is obtained by adjusting the length of the resonators and the length of the supports. Note that this structure offers a high degree of design flexibility in terms of shape. Indeed, the structure can be designed straight or bent as in Fig. P14 to obtain a more compact structure. Like the other filters presented in this section, this structure can be easily made with AM, whereas it is relatively complex to build with traditional subtractive technologies. The main characteristics of some of the filters in plastic AM presented in this paper are summarized in Table P01.

Exploitation of the free-form capability of AM has also been investigated in view of the miniaturization of low-frequency filters by applying vat photopolymerization techniques, such as SLA and DLP, to

ceramic materials. In [Carceller01], DLP was used to build an X-band two-pole dielectric-resonator filter in a single alumina part, which was subsequently externally metal plated. The main advantage of this solution is not having dielectric rods mounted within metal cavities, thus leading to a more robust device, especially with respect to temperature variations. The possibility of manufacturing ceramic parts with complex shapes was also exploited in [Perigaud01] in order to develop a tunable filter working in the Ku-band. The frequency tunability of the filter is based on the synchronous rotation of zirconia perturbers inserted in the waveguide resonators. The optimization of the filter performance in terms of constant bandwidth over a wide tuning range was achieved by manufacturing the zirconia inserts with complex shapes through SLA.

Conclusions

This article shows that additive manufacturing technologies are beginning to be successfully applied in the development of high-performance filters with novel topologies working from a few GHz to approximately 20-30 GHz (K, Ka bands). Examples are filters with shaped-waveguide resonators directly built in aluminum through selective laser melting [Booth01], and stacked-cavity filters printed by stereolithography [Chappell04]. The unique free-form feature of AM processes has been exploited for the successful implementation of filter layouts that are at the edge of the capacity of conventional machining, such as mushroom cavity filters coupled via suspended wires [Tomassoni08] and the integration of multiple RF functionalities in monolithic filtering structures [Peverini04]. In recent years, exploitation of the most accurate AM processes, such as SLA [Shang01] and micro SLM [Salek01], have made possible the application of AM technologies at higher frequencies, such as the W band.

Research on AM for RF components is currently focused on the following main aspects: i) The optimization of AM processes for RF applications (*e.g.*, surface roughness, metallization, selection of proper materials); ii) Re-design of canonical RF architectures according to guidelines for AM-oriented design (*e.g.*, smooth surfaces, suited geometries); iii) The development of new classes of components that exploit the high flexibility of AM in manufacturing new geometries that are difficult or impossible to manufacture via conventional subtracting techniques. Most current research focuses on just one of these aspects. It is the authors' opinion that the development of filters with increased performance will benefit from research activities that are focused on all of the aforementioned aspects and that are based on a concurrent engineering approach that encompasses multiple competencies, among them RF engineering, material science, and mechanical and production engineering. As an example, selective laser melting has already been proven to be suitable for manufacturing all-metal filters with adequate electrical surface resistivity (*e.g.*, 10-20 μΩcm for AlSi10Mg alloy without additional coating), surface roughness as low as 5μm after shot-peening of the internal faces, and dimensional accuracy on the order of 30-60 μm. However, it must be noted that all of these properties depend strongly on the process and post-process parameters as well as the filter geometry. For example, the staircase effect arising from the discretization of the filter profile along the building direction affects both the surface roughness and the dimensional accuracy. As a rule of thumb, the faces of the internal channels should be inclined at least 45 degrees. Indeed, if filter architectures are redesigned according to this recommendation, no supporting structures for the internal surfaces are needed and the risk of warping and cracks is minimized. Other important process parameters to be fine-tuned are the compensation factors that account for the shrinkage of the parts due to thermal stresses, and the beam offset that compensates for the enlargement of the effective spot size due to thermal diffusion. Similar considerations hold for polymer-based AM processes, like SLA and FDM. In sum we anticipate that steady improvements in

AM processes, materials, and post-processings pave the way for these technologies to become widely adopted in the production of RF components, including filters, for a variety of application domains (*e.g.*, SatCom, automotive radar, IoT), for which the capability of manufacturing light and customizable components makes AM technologies very attractive.

References

[ASTM01] F2792-12a, "Standard terminology for additive manufacturing technologies", STM International, West Conshohocken, PA, USA, 2012

[Wohlers01] T. Wohlers, "Additive manufacturing and 3D printing state of the industry," Fort Collins, CO, USA: Wohlers Assoc. Inc., 2018

[Hao01] L. Hao, D. Raymond, G. Strano, and S. Dadbakhsh, "Enhancing the sustainability of additive manufacturing," in *5th Int. Conf. on Responsive Manufacturing - Green Manufacturing (ICRM 2010)*, Ningbo, China, 2010, doi: 10.1049/cp.2010.0462

[Manfredi01] D. Manfredi, *et al.*, "Additive manufacturing of Al alloys and aluminium matrix composites (AMCs)," in *Light Metal Alloys Applications*, Waldemar A. Monteiro: InTech, 2014. pp. 3-34

[Guo01] N. Guo and M. C. Leu, "Additive manufacturing: technology, applications and research needs," *Front. Mech. Eng.,* vol. 8, no. 3, pp. 215-243, Sep. 2013

[Gibson01] I. Gibson, B. Stucker and D. W. Rosen, *Additive manufacturing technologies: Rapid prototyping to direct digital manufacturing*: Springer, 2010

[Calignano01] F. Calignano, *et al.*, “Overview on additive manufacturing technologies,” *Proc. IEEE*, vol. 105, no 4, pp. 593-612, Jan. 2017

[Hinczewski01] C. Hinczewski, S. Corbel, T. Chartier, "Ceramic suspensions suitable for stereolithography", *J. Eur. Ceram. Soc.*, vol. 18, no. 6, pp. 583-590, 1998

[Booth01] P. Booth, J. Gilmore, E. V. Lluch and M. Harvey, "Enhancements to satellite feed chain performance, testing and lead-times using additive manufacturing," in *10th European Conf. on Antennas and Propagation (EuCAP)*, Davos, Switzerland, 2016, pp. 1-5, doi: 10.1109/EuCAP.2016.7481882

[Addamo01] G. Addamo *et al.*, "3-D Printing of high-performance feed horns from Ku- to V-bands", *IEEE Antennas Wireless Propag. Lett.*, vol. 17, no. 11, pp. 2036-2040, Nov. 2018

[Chio01] T. Chio, G. Huang and S. Zhou, "Application of direct metal laser sintering to waveguide-based passive microwave components, antennas, and antenna arrays," *Proc. IEEE*, vol. 105, no. 4, pp. 632-644, Apr. 2017

[Kilian01] M. Kilian, C. Hartwanger, M. Schneider and M. Hatzenbichler, "Waveguide components for space applications manufactured by additive manufacturing technology," *IET Microw. Antenna P.*, vol. 11, no. 14, pp. 1949-1954, Nov. 2017

[Addamo02] G. Addamo *et al.*, "Additive manufacturing of Ka-Band dual-polarization waveguide components," *IEEE Trans. Microw. Theory Tech.*, vol. 66, no. 8, pp. 3589-3596, Aug. 2018

[Crestvolant01] V. Tornielli di Crestvolant, P. Martin Iglesias and M. J. Lancaster, "Advanced Butler matrices with integrated bandpass filter functions," *IEEE Trans. Microw. Theory Tech.*, vol. 63, no. 10, pp. 3433-3444, Oct. 2015

[Lorente01] M. M. Mendoza, A. Z. Petersson, L. Pambaguian, A. A. Melcon, and C. Ernst, "Single part microwave filters made from selective laser melting," in *2009 European Microwave Conf. (EuMC)*, Rome, Italy, 2009, pp. 1421-1424, doi: 10.23919/EUMC.2009.5296127

[Booth02] P. Booth and E. V. Lluch, "Enhancing the performance of waveguide filters using additive manufacturing", *Proc. IEEE*, vol. 105, no. 4, pp. 613-619, Apr. 2017

[Booth03] P. A. Booth and E. Valles Lluch, "Realising advanced waveguide bandpass filters using additive manufacturing," *IET Microw. Antenna P.*, vol. 11, no. 14, pp. 1943-1948, Nov. 2017

[Sattler01] S. W. Sattler, F. Gentili, R. Teschl and W. Bösch, "Direct metal printed 4th order stepped impedance filter in the C/X Band," in *2018 IEEE/MTT-S Int.l Microw. Symp. (IMS)*, Philadelphia, USA, Jun. 2018, pp. 145-148, doi: 10.1109/MWSYM.2018.8439567

[Peverini01] O. A. Peverini *et al*., "Manufacturing of waveguide components for SatCom through selective laser melting," in *11th European Conf. on Antennas and Propagation (EUCAP)*, Paris, France, 2017, pp. 563-566, doi: 10.23919/EuCAP.2017.7928301

[Peverini02] O. A. Peverini *et al*., "Additive manufacturing of Ku/K-band waveguide filters: a comparative analysis among selective-laser melting and stereo-lithography," *IET Microw., Antenna P.*, vol. 11, no. 14, pp. 1936-1942, Nov. 2017

[Peverini03] O. A. Peverini *et al*., "Enhanced topology of E-plane resonators for high-power satellite applications," *IEEE Trans. Microw. Theory Tech.*, vol. 63, no. 10, pp. 3361-3373, Oct. 2015

[Peverini04] O. A. Peverini *et al*., "Selective laser melting manufacturing of microwave waveguide devices," *Proc. IEEE*, vol. 105, no. 4, pp. 620-631, Apr. 2017

[Calignano02] F. Calignano, *et al.* “Influence of process parameters on surface roughness of aluminum parts produced by DMLS,” Int. J. Adv. Manuf. Techn., vol. 67, pp. 2743-2751, 2013

[Zhang01] B. Zhang and H. Zirath, "3D printed iris bandpass filters for millimetre-wave applications," *Electronic Lett.*, vol. 51, no. 22, pp. 1791-1793, Oct. 2015

[Salek01] M. Salek *et al*., "W-Band waveguide bandpass filters fabricated by micro laser sintering," *IEEE Trans. Circuits Syst., II, Exp. Briefs*, vol. 66, no. 1, pp. 61-65, Jan. 2019

[Peverini05] O. A. Peverini *et al*., "Integration of an H -plane bend, a twist, and a filter in Ku/K-band through additive manufacturing," *IEEE Trans. Microw. Theory Tech.*, vol. 66, no. 5, pp. 2210-2219, May 2018

[Montejio01] J. R. Montejo-Garai, I. O. Saracho-Pantoja, C. A. Leal-Sevillano, J. A. Ruiz-Cruz and J. M. Rebollar, "Design of microwave waveguide devices for space and ground application implemented by additive manufacturing," in *2015 Int. Conf. on Electromagnetics in Advanced Applications (ICEAA),* Turin, Italy, 2015, pp. 325-328, doi: 10.1109/ICEAA.2015.7297128

[Delhote01] A. Périgaud, S. Bila, O. Tantot, N. Delhote and S. Verdeyme, "3D printing of microwave passive components by different additive manufacturing technologies," in *2016 IEEE MTT-S Int. Microwave Workshop Series on Advanced Materials and Processes for RF and THz Applications (IMWS-AMP),* Chengdu, China, 2016, pp. 1-4, doi: 10.1109/IMWS-AMP.2016.7588328

[Jankovic01] U. Jankovic, N. Mohottige, D. Budimir and O. Glubokov, "Hybrid manufactured waveguide resonators and filters for mm-wave applications," *2017 IEEE MTT-S Int. Microwave Workshop Series on Advanced Materials and Processes for RF and THz Applications (IMWS-AMP),* Pavia, Italy, 2017, doi: 10.1109/IMWS-AMP.2017.8247360

[Massoni01] E. Massoni, *et al.*, "3D printing and metalization methodology for high dielectric resonator waveguide microwave filters", in *2017 IEEE MTT-S International*

Microwave Workshop Series on Advanced Materials and Processes for RF and THz Applications (IMWS-AMP), Pavia, Italy, 2017, doi: 10.1109/IMWS-AMP.2017.8247417

[Tomassoni01] M. Bozzi, C. Tomassoni, L. Perregrini, R. Bahr, and M. Tentzeris, "Additive manufacturing of substrate integrated waveguide components," in *2016 IEEE MTT-S Int. Microwave Workshop Series on Advanced Materials and Processes for RF and THz Applications (IMWS-AMP)*, Chengdu, China, 2016, doi: 10.1109/IMWS-AMP.2016.7588329

[Tomassoni02] C. Tomassoni, R. Bahr, M. Tentzeris, M. Bozzi, L. Perregrini, "3D printed substrate integrated waveguide filters with locally controlled dielectric permittivity", in *46th European Microwave Conf. (EuMC),* London, UK, 2016, pp. 253-256, doi: 10.1109/EuMC.2016.7824326

[Tomassoni03] C. Tomassoni, M. Bozzi, M. Dionigi, G. Venanzoni, L. Perregrini, R. Sorrentino, "Additive manufacturing of microwave components: Different approaches and methodologies", in *2017 Int. Conf. on Electromagnetics in Advanced Applications (ICEAA), 11-15 Sept. 2017,* Verona, Italy

[Chappell01] Bosui Liu, Xun Gong, and W. J. Chappell, "Layer-by-layer polymer stereolithography fabrication for three-dimensional RF components," in *2004 IEEE MTT-S Int. Microwave Symposium Digest,* Fort Worth, TX, USA, 2004, pp. 481-484, doi: 10.1109/MWSYM.2004.1336017

[Chappell02] Xun Gong, Bosui Liu, L. P. B. Katehi and W. J. Chappell "Laser-based polymer stereolithography of vertically integrated narrow bandpass filters operating in K

band," in *2004 IEEE MTT-S Int. Microwave Symposium Digest*, Fort Worth, TX, USA, 2004, pp. 425-428, doi: 10.1109/MWSYM.2004.1336000

[Chappell03] L. Hao, D. Raymond, G. Strano and S. Dadbakhsh, "Enhancing the sustainability of additive manufacturing," in *5th Int. Conf. on Responsive Manufacturing - Green Manufacturing (ICRM 2010),* Ningbo, China, 2010, pp. 390-395, doi: 10.1049/cp.2010.0462

[Chappell04] J. Maas, B. Liu, S. Hajela, Y. Huang, X. Gong, and W. J. Chappell, "Laser-based layer-by-layer polymer stereolithography for high-frequency applications," *Proc. IEEE*, vol. 105, no. 4, pp. 645-654, Apr. 2017

[Tomassoni04] G. Venanzoni, M. Dionigi, C. Tomassoni, D. Eleonori, and R. Sorrentino, "3D printing of X band waveguide resonators and filters," in *2017 XXXIInd General Assembly and Scientific Symp. of the International Union of Radio Science (URSI GASS)*, Montreal, Canada, 2017, pp. 1-2, doi: 10.23919/URSIGASS.2017.8105407.

[Dauria01] M. D'Auria, *et al*., "3-D printed metal-pipe rectangular waveguides," *IEEE Trans. Compon. Packag. Manuf. Technol.*, vol. 5, no. 9, pp. 1339-1349, Sep. 2015.

[Shang01] X. Shang *et al*., "W-Band waveguide filters fabricated by laser micromachining and 3-D Printing," *IEEE Trans. Microw. Theory Tech.*, vol. 64, no. 8, pp. 2572-2580, Aug. 2016.

[Cai01] Fan Cai, Wasif Tanveer Khan and J. Papapolymerou, "A low loss X-band filter using 3-D polyjet technology," in *2015 IEEE MTT-S Int. Microwave Symp.*, Phoenix, AZ, USA, 2015, pp. 1-4, doi: 10.1109/MWSYM.2015.7166895

[Park01] K. Y. Park, M. I. M. Ghazali, N. Wiwatcharagoses and P. Chahal, "Thick 3D printed RF components: Transmission lines and bandpass filters," in *2018 IEEE 68th*

Electronic Components and Technology Conf. (ECTC), San Diego, CA, USA, 2018, pp. 2186-2191.doi: 10.1109/ECTC.2018.00328

[Lucyszyn01] B. Al-Juboori, *et al*., "Lightweight and low-Loss 3-D printed millimeter-wave bandpass filter based on gap-waveguide," *IEEE Access*, vol. 7, pp. 2624-2632, 2019.

[Craton01] M. T. Craton, J. Sorocki, I. Piekarz, S. Gruszczynski, K. Wincza, and J. Papapolymerou, "Realization of fully 3D printed W-band bandpass filters using Aerosol jet printing technology," in *2018 48th European Microwave Conf. (EuMC),* Madrid, 2018, pp. 1013-1016, doi: 10.23919/EuMC.2018.8541416

[Tomassoni05] M. Dionigi, C. Tomassoni, G. Venanzoni and R. Sorrentino, "Simple high-performance metal-plating procedure for stereolithographically 3-D-printed waveguide components," *IEEE Microw. Wireless Compon. Lett.*, vol. 27, no. 11, pp. 953-955, Nov. 2017

[Shang02] C. Guo, X. Shang, M. J. Lancaster and J. Xu, "A 3-D printed lightweight X-band waveguide filter based on spherical resonators," *IEEE Microw. Wireless Compon. Lett.,* vol. 25, no. 7, pp. 442-444, Jul. 2015.

[Guo02] C. Guo, X. Shang, J. Li, M. J. Lancaster and J. Xu, "3-D printed lightweight microwave waveguide devices," in *2016 IEEE 5th Asia-Pacific Conf. on Antennas and Propagation (APCAP)*, Kaohsiung, Taiwan, 2016, pp. 47-48, doi: 10.1109/APCAP.2016.7843092.

[Shang03] C. Guo, X. Shang, J. Li, F. Zhang, M. J. Lancaster and J. Xu, "A lightweight 3-D printed X-band bandpass filter based on spherical dual-mode resonators," in *IEEE Microw. Wireless Compon. Lett.*, vol. 26, no. 8, pp. 568-570, Aug. 2016.

[Wang01] Y. Li, J. Li, M. Zhang, H. Wang, J. Xu and S. Xiao, "A monolithic stereolithography 3-D printed Ka-band spherical resonator bandpass filter," in *2018 IEEE Radio and Wireless Symp. (RWS)*, Anaheim, CA, USA, 2018, pp. 56-59, doi: 10.1109/RWS.2018.8304945

[Yuan01] J. Li, C. Guo, L. Mao, J. Xiang, G. Huang and T. Yuan, "Monolithically 3-D printed hemispherical resonator waveguide filters with improved out-of-band rejections," *IEEE Access*, vol. 6, pp. 57030-57048, 2018

[Shang04] X. Shang, J. Li, C. Guo, M. J. Lancaster and J. Xu, "3-D printed filter based on helical resonators with variable width," in *2017 IEEE MTT-S Int. Microwave Symp. (IMS)*, Honololu, HI, USA, 2017, pp. 1587-1590, doi: 10.1109/MWSYM.2017.8058936

[Delhote02] A. Perigaud, O. Tantot, N. Delhote, S. Bila, S. Verdeyme, and D. Baillargeat, "Continuously tunable filter made by additive manufacturing using a 3D spiral ribbon," *2017 IEEE MTT-S Int. Microwave Workshop Series on Advanced Materials and Processes for RF and THz Applications (IMWS-AMP)*, Pavia, Italy, 2017, pp. 1-3, doi: 10.1109/IMWS-AMP.2017.8247372

[Tomassoni06] G. Venanzoni, C. Tomassoni, M. Dionigi, R. Sorrentino, “Stereolitographic 3D Printing of Compact Quasi-Elliptical Filters”, *IEEE MTT-S Int. Microwave Workshop Series on Advanced Materials and Processes (IMWS-AMP 2017)*, Pavia, Italy, 2017, pp. 1-3, doi: 10.1109/IMWS-AMP.2017.8247388

[Tomassoni07] C. Tomassoni, G. Venanzoni, M. Dionigi and R. Sorrentino, "Compact doublet structure for quasi-elliptical filters using stereolitographic 3D printing," *2017 47th*

European Microwave Conf. (EuMC), Nuremberg, Germany, 2017, pp. 993-996, doi: 10.23919/EuMC.2017.8231013

[Tomassoni08] C. Tomassoni, G. Venanzoni, M. Dionigi and R. Sorrentino, "Compact quasi-elliptic filters with mushroom-shaped resonators manufactured with 3-D printer," *IEEE Trans. Microw. Theory Tech*, vol. 66, no. 8, pp. 3579-3588, Aug. 2018

[Venanzoni01] G. Venanzoni, M. Dionigi, C. Tomassoni and R. Sorrentino, "3-D-printed quasi-elliptical evanescent mode filter using mixed electromagnetic coupling," *IEEE Microw. Wireless Compon. Lett.*, vol. 28, no. 6, pp. 497-499, Jun. 2018

[Tomassoni09] C. Tomassoni, G. Venanzoni, M. Dionigi and R. Sorrentino, "Additive manufacturing of a very compact doublet structure with asymmetric filtering function", in *IEEE MTT-S Int. Microwave Workshop Series on Advanced Materials and Processes for RF and THz Applications (IMWS-AMP 2018),* Ann Arbor, MI, USA, 2018, pp. 1-3, doi: 10.1109/IMWS-AMP.2018.8457127

[Tomassoni10] C. Tomassoni, G. Venanzoni, M. Dionigi and R. Sorrentino, "A very compact 3D-printed doublet structure based on a double iris and a pair of slanting rods," in *2018 IEEE/MTT-S Int. Microwave Symp. (IMS)*, Philadelphia, PA, USA, 2018, pp. 1103-1105, doi: 10.1109/MWSYM.2018.8439368

[Venanzoni02] G. Venanzoni, M. Dionigi, C. Tomassoni and R. Sorrentino, "Design of a compact 3D printed coaxial filter", in *48th European Microwave Conf.*, Madrid, Spain, 2018, pp. 280-283, doi: 10.23919/EuMC.2018.8541590

[Carceller01] C. Carceller, F. Gentili, D. Reichartzeder, W. Bösch and M. Schwentenwein, "Development of monoblock TM dielectric resonator filters with additive

manufacturing", in *IET Microw. Antenna P.*, vol. 11, no. 14, pp. 1992-1996, Nov. 2017

[Perigaud01] A. Périgaud, *et al.*, "Continuously tuned Ku-Band cavity filter based on dielectric perturbers made by ceramic additive manufacturing for space applications", *Proc. IEEE*, vol. 105, no. 4, pp. 677-687, Apr. 2017

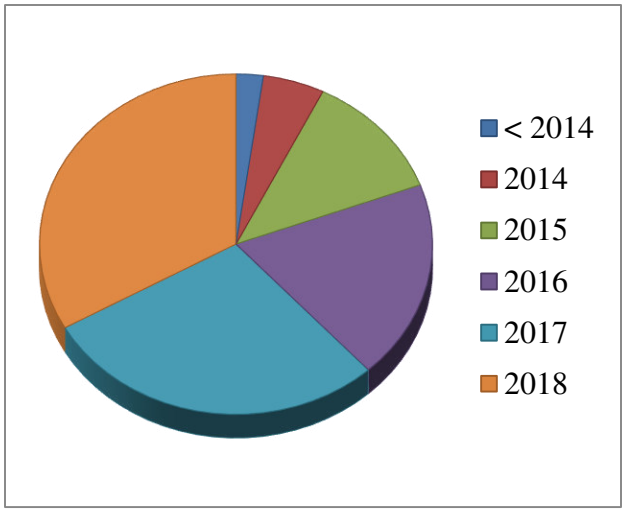

Figure A01. Numbers of publications on 3D printing of microwave components in IEEE journals and conferences, pre-2014 through 2018 (source IEEE Xplore Digital Library)

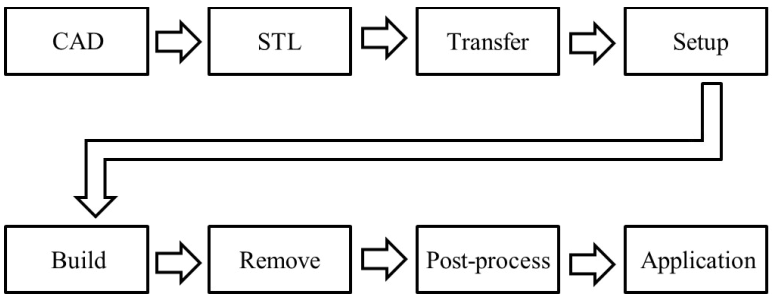

Figure A02. Workflow of a generic additive manufacturing process

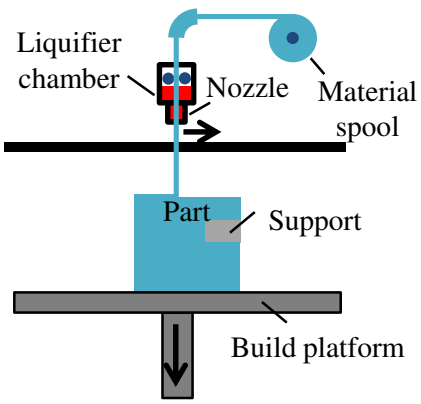

Figure A03. Generic material extrusion process

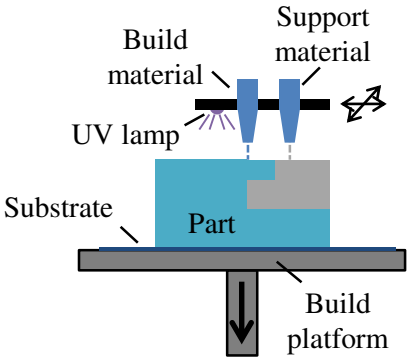

Figure A04. Generic material jetting process

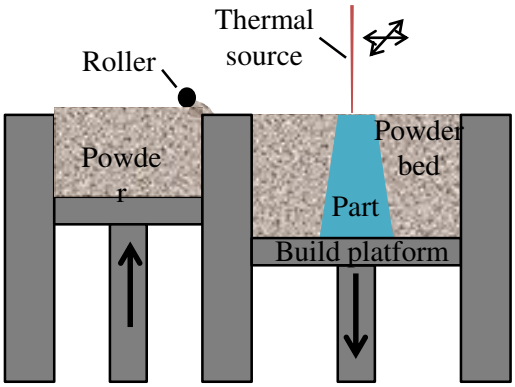

Figure A05. Generic powder bed fusion process

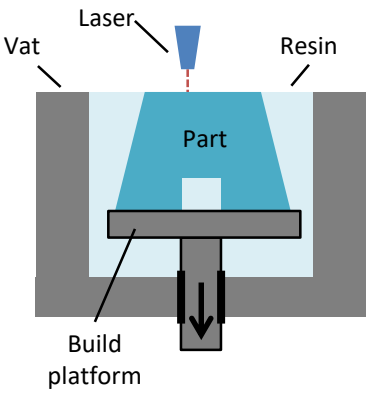

Figure A06. Generic vat photopolymerization process

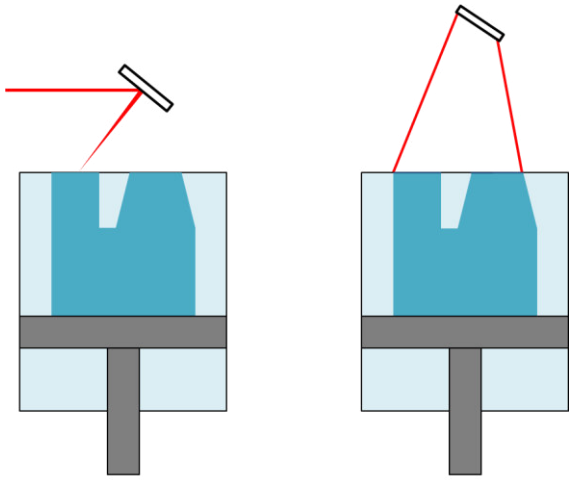

Figure A07. Scanning schemes used in vat photopolymerization. (a) Vector scan. (b) Mask projection.

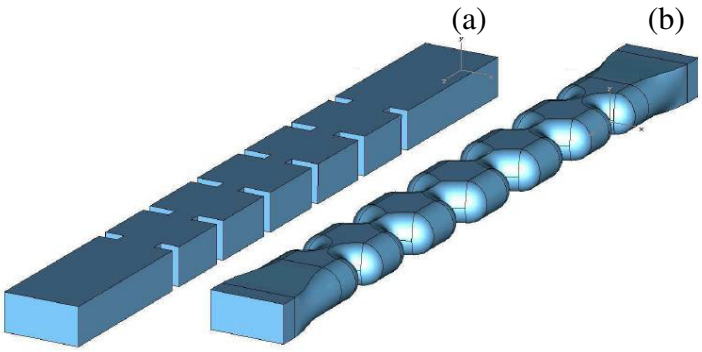

Figure B01. 3D view of the inner waveguide structure of the Ku-band filters developed in [Lorente01]. (a) Standard layout. (b) Shaped layout.

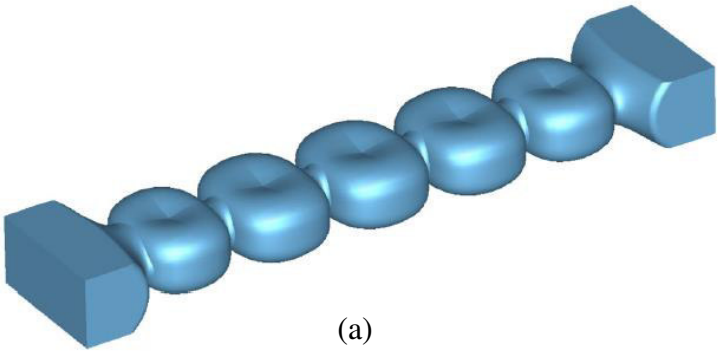

(a)

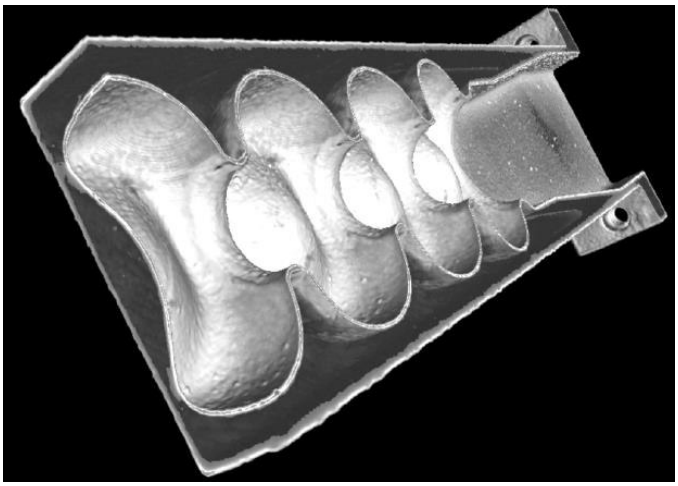

(b)

Figure B02. 3D view of the inner waveguide structure of the Ku-band filter developed in [Booth02]. (a) CAD model. (b) Computed tomography scan.

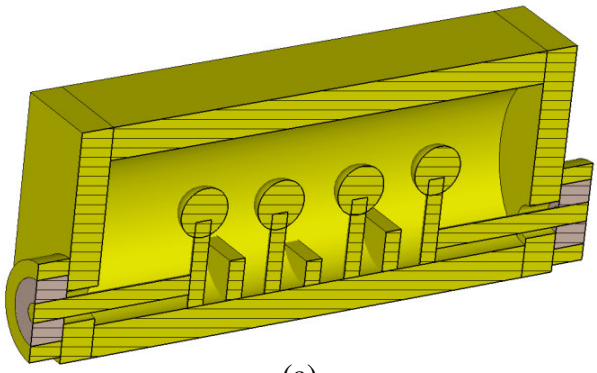

(a)

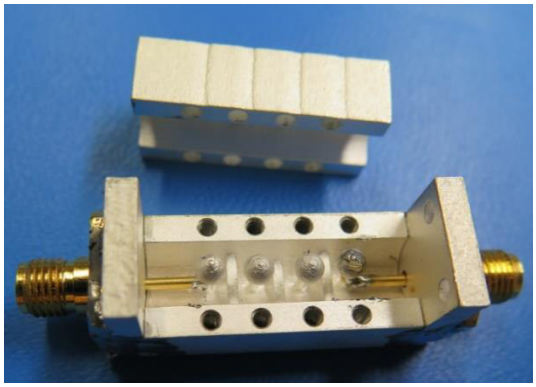

(b)

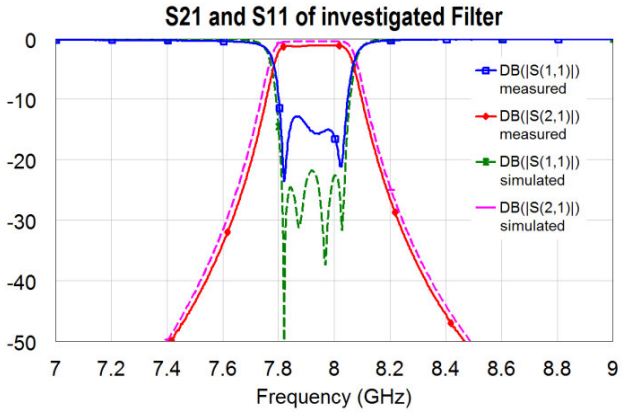

(c)

Figure B03. Stepped impedance filter developed in [Sattler01]. (a) Cut view of the CAD model showing the modified mushroom resonators. (b) Prototype manufactured through selective laser melting. (c) Comparison between measured and predicted scattering coefficients.

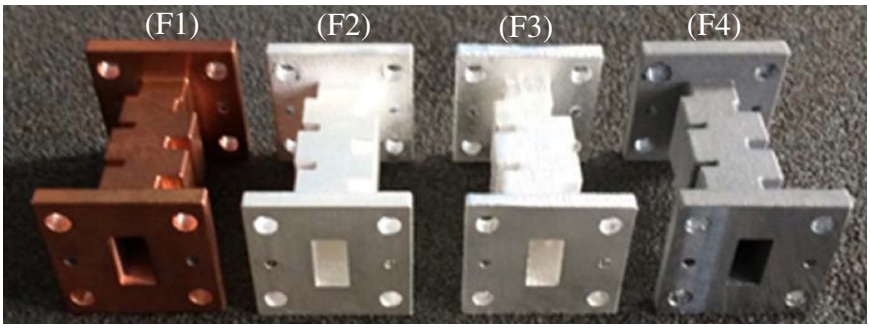

(a)

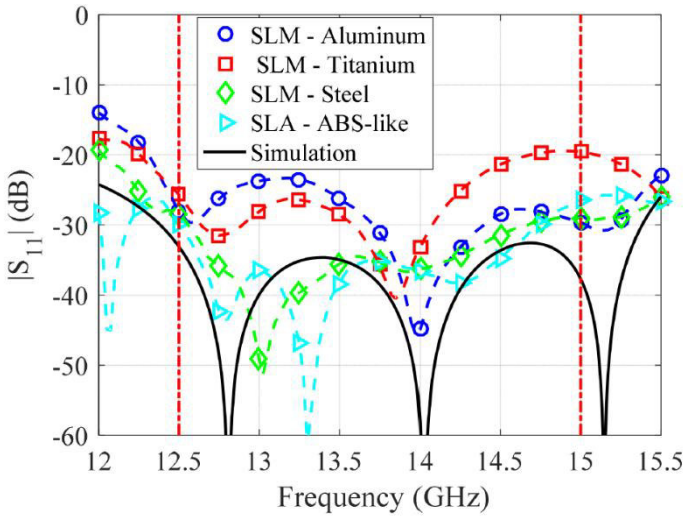

(b)

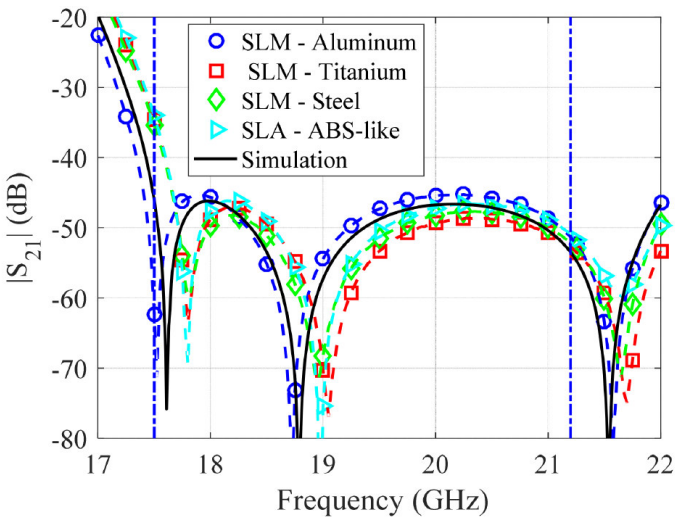

(c)

Figure B04. Comparative analysis reported in [Peverini01] among Ku/K-band filters printed with SLM and SLA. F1: SLA with copper plating. F2: SLM in maraging steel with silver plating. F3: SLM in titanium with silver plating. F4: SLM in aluminum.
(a) In-band reflection coefficient. (b) Out-of-band transmission coefficient.

(a)

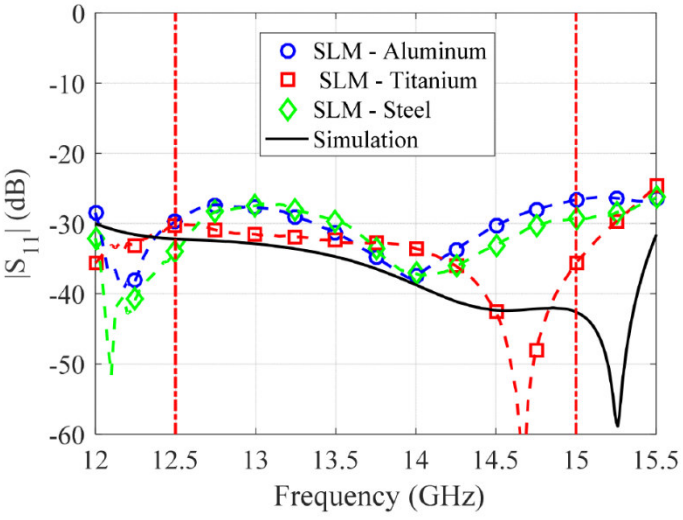

(b)

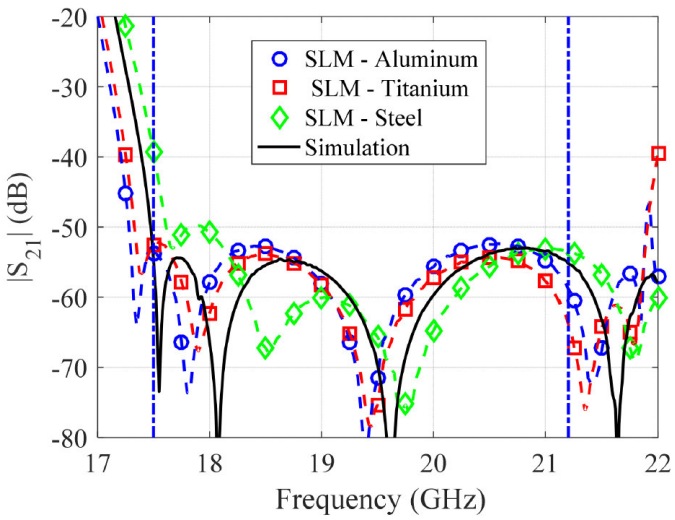

(c)

Figure B05. Comparative analysis reported in [Peverini01] among Ku/K-band filters printed with SLM and SLA. F1: SLA with copper plating. F2: SLM in maraging steel without silver plating. F3: SLM in titanium without silver plating. F4: SLM in aluminum.
(a) In-band reflection coefficient. (b) Out-of-band transmission coefficient.

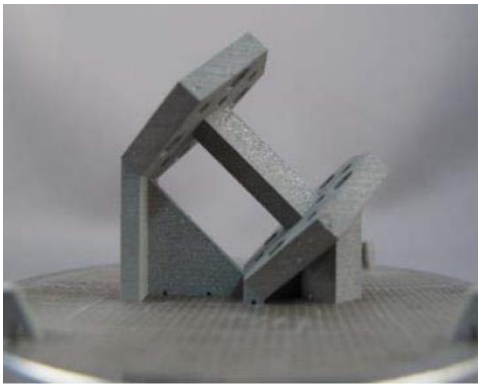

(a)

(b)

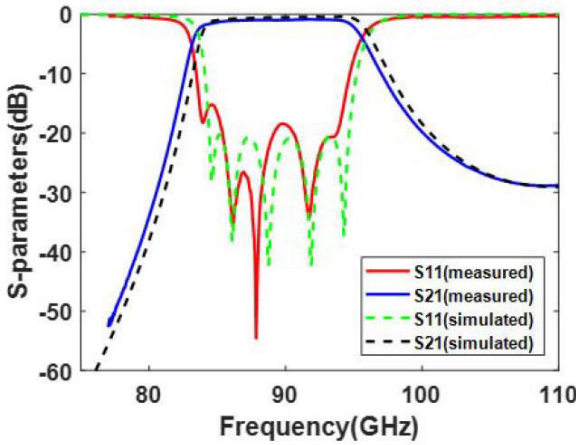

(c)

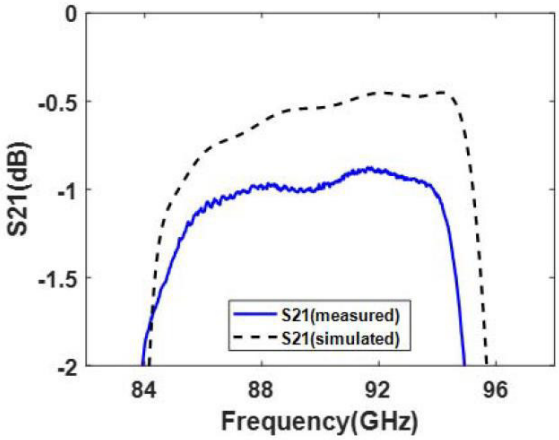

(d)

Figure B06. W-band passband filter developed in [Salek01]
(a) Prototype as built. (b) Prototype after copper plating. (c) Scattering coefficients. (d) Insertion loss

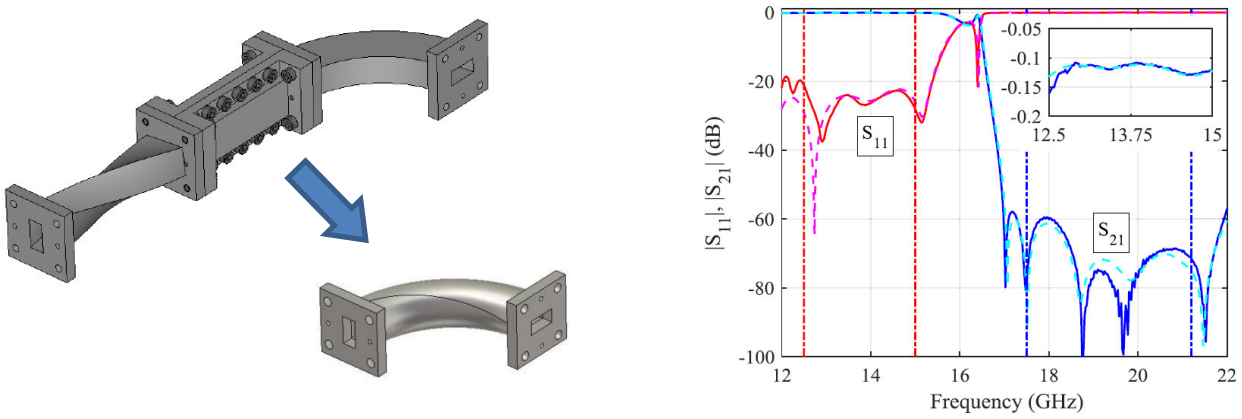

(a) (b)

Figure B07. Integration of a filter, a twist, and an H-plane bend in a miniaturized metal part through SLM [Peverini04]. (a) CAD model of the initial waveguide sub-system and of the miniaturized assembly. (b) Comparison between the measured and predicted scattering coefficients.

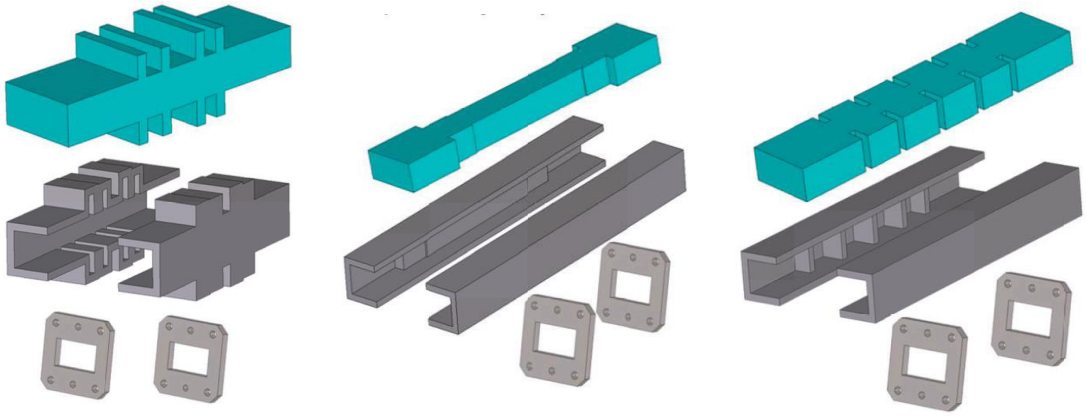

(a) (b) (c)

Figure P01. Example of filters fabricated with FDM technology [Montejio01]. (a) Corrugated low-pass filter. (b) High-pass filter. (c) Band-pass filter

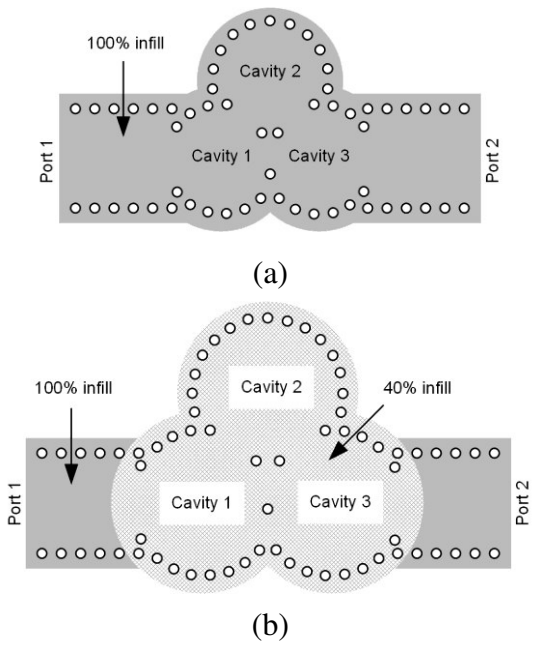

Figure P02. Substrate integrated waveguide filter with 3D printed dielectric layer [Tomassoni01]. The infill percentage inside the cavities is different in order to change the dielectric constant and losses. (a) 100% infill. (b) 40% infill.

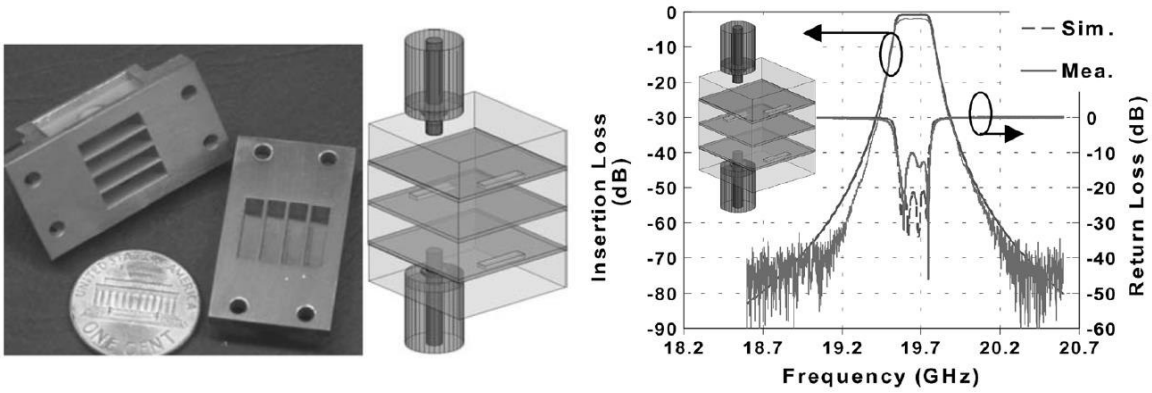

(a) (b)

Figure P03. Four-cavity waveguide filter fabricated with SLA technology [Chappell04]. (a) picture of the filter with internal view. (b) Measurements and simulations.

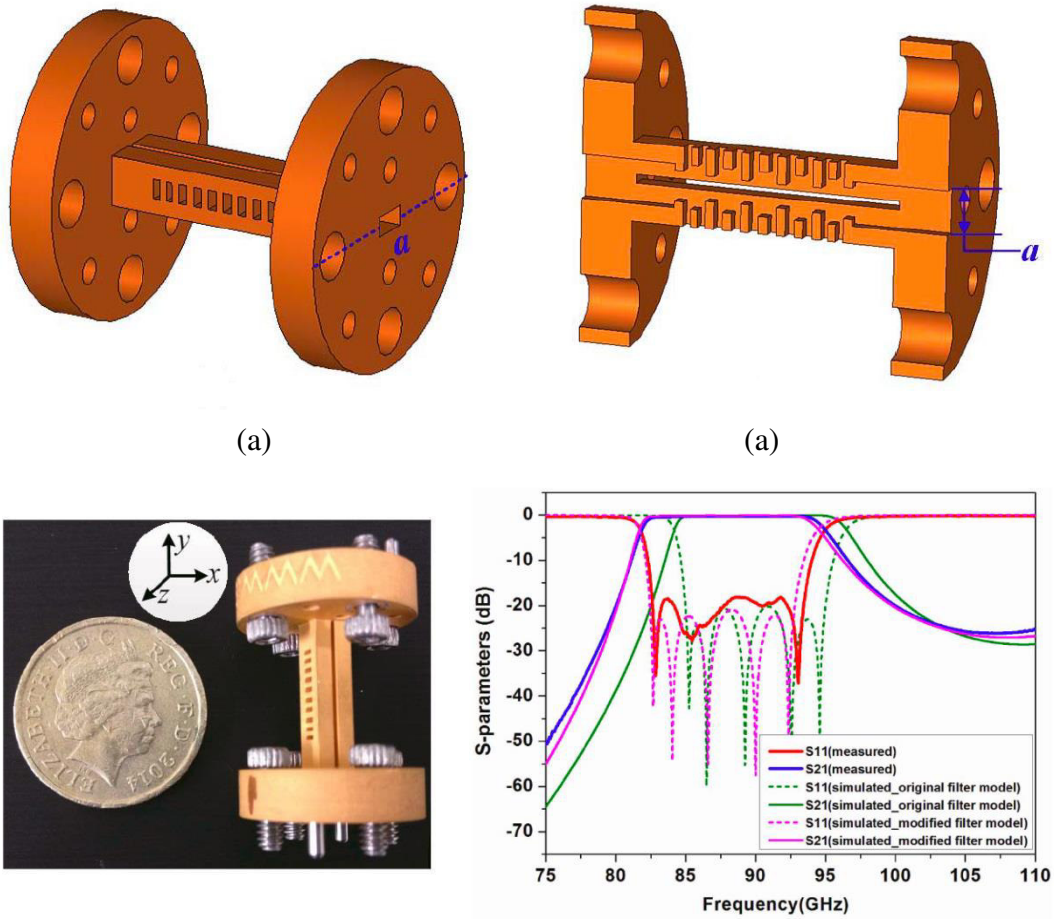

(a) (a)

(c) (d)

Figure P05. W-band waveguide filter [Shang01]. (a) External view. (b) Cut view. (c) Photograph of the filter. (d) Measurements and simulations.

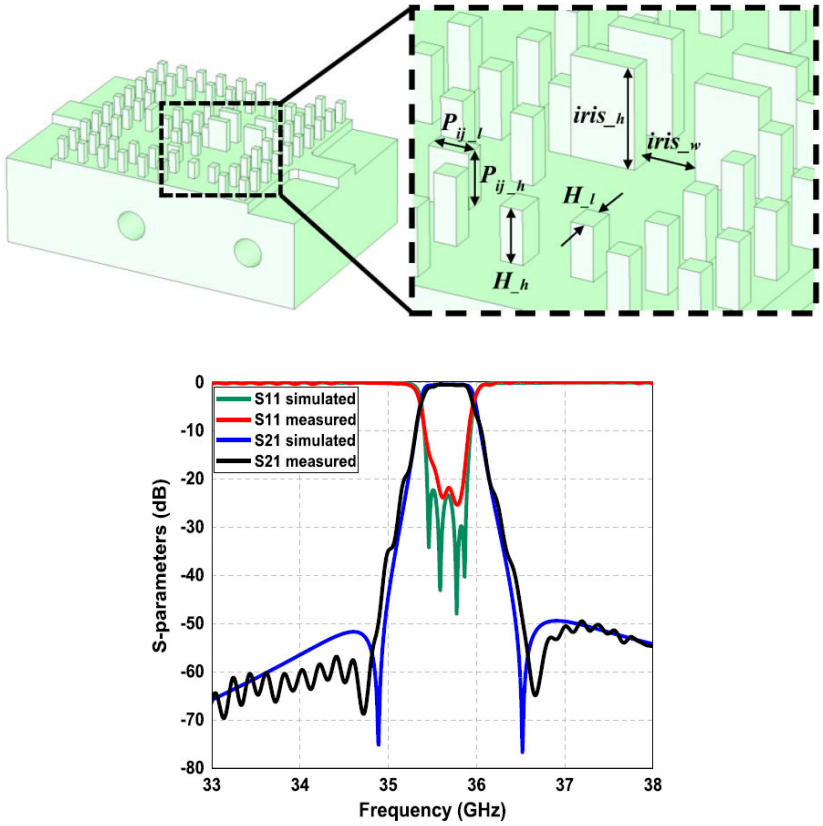

Figure P06. Gap waveguide filter working in the Ka band [LUCYSZYN01]

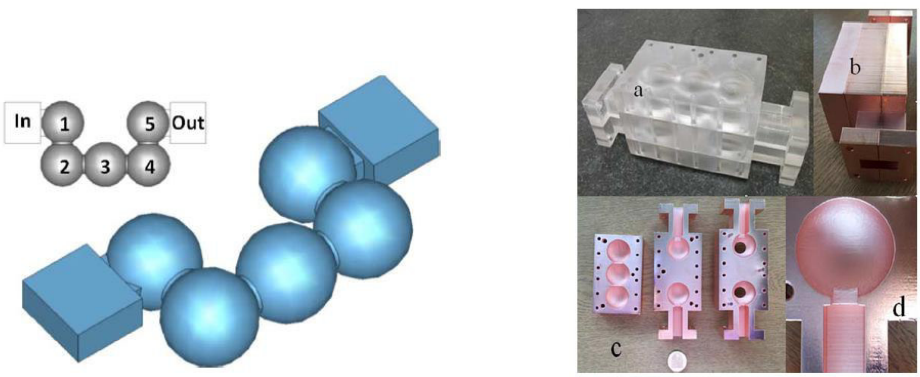

Figure P07. Five-cavity filter that uses single mode spherical resonators [Shang02].

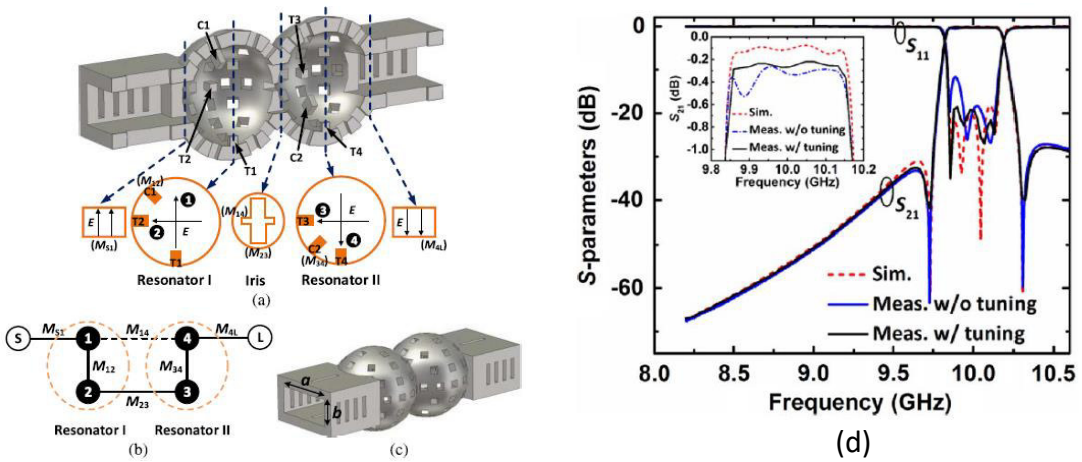

Figure P08. Dual-mode spherical cavity filter [Guo01][Shang03]. (a) Inside view. (b) Coupling scheme. (c) 3D view. (d) Measurements and simulations.

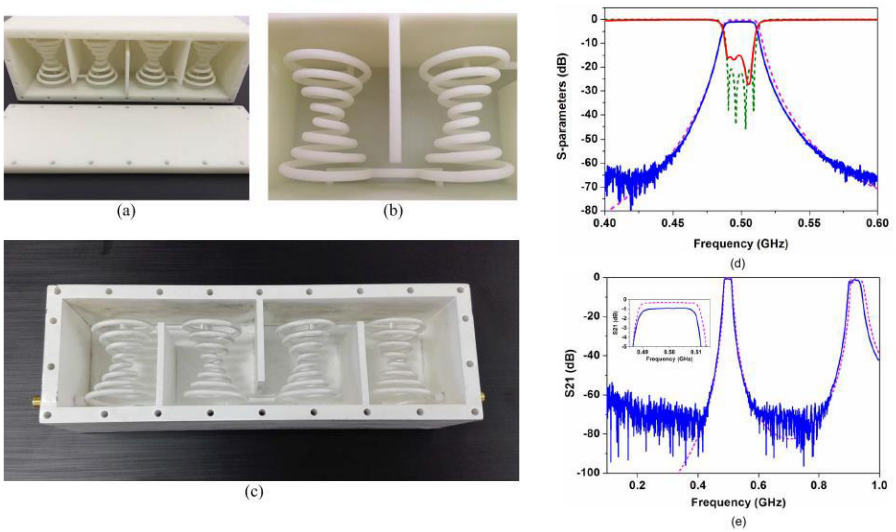

Figure P09. Helical resonator filter, working in the UHF band [Shang04].

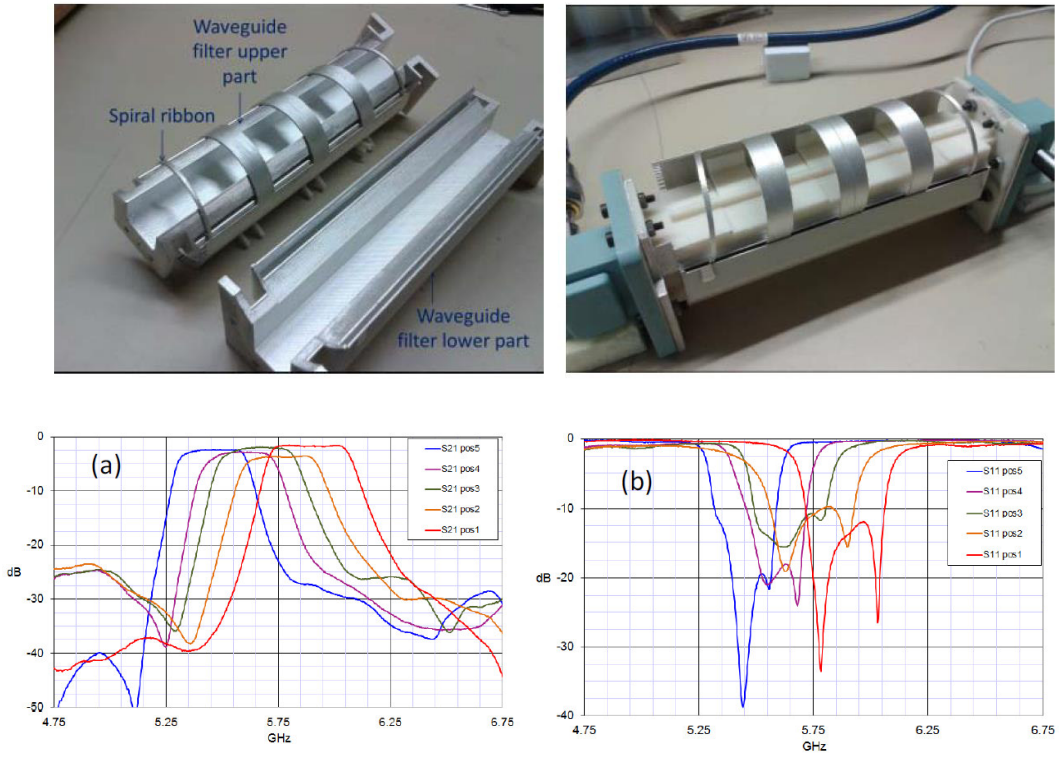

Figure P10. Tunable E-plane filter with a rotating spiral ribbon to change the band [Delhote02]. The experimental results are for different positions of the spiral ribbon. (a) Transmission coefficient. (b) Reflection coefficient

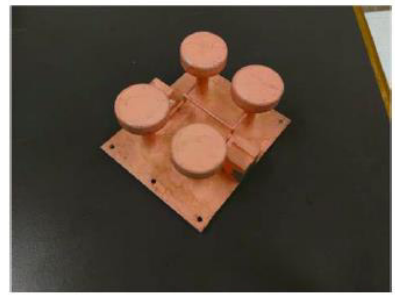

(a)

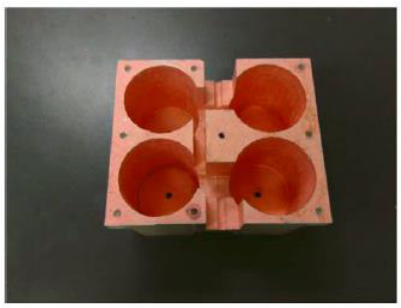

(b)

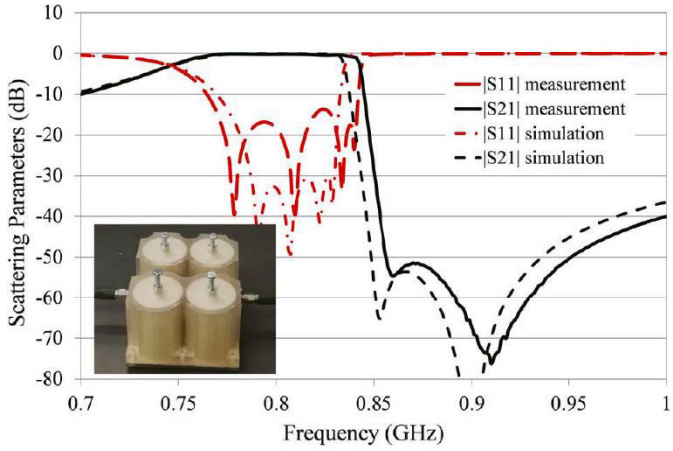

(c)

Figure P11. Four-pole "mushroom" filter working in the UHF band [Tomassoni08]. (a) Main body. (b) Cover. (c) Comparison between measurements and simulations.

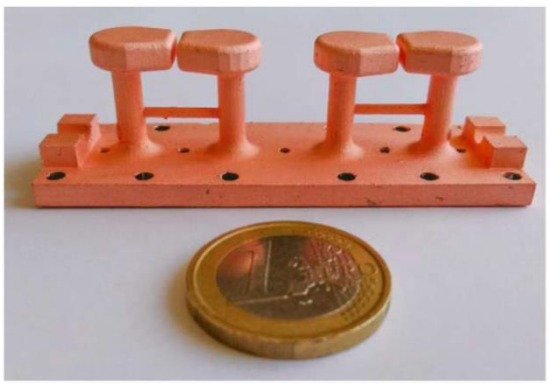

(a)

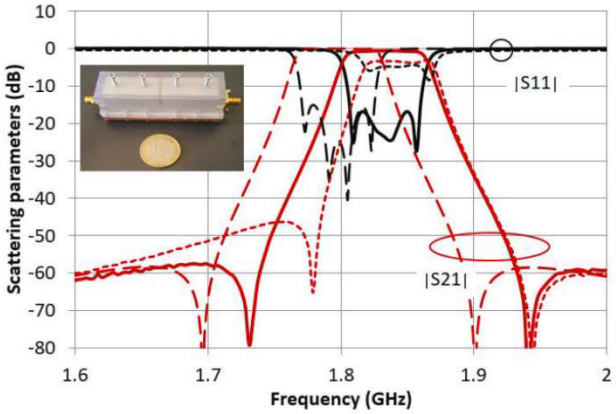

(b)

Figure P12. Four-pole "mushroom" filter with mixed electric and magnetic coupling working at 1.8 GHz [Venanzoni01]. (a) Photo of the main body of the filter. (b) Comparison among simulations (dashed curves), measurements without tuning (dotted curves), and measurements with tuning (continuous)

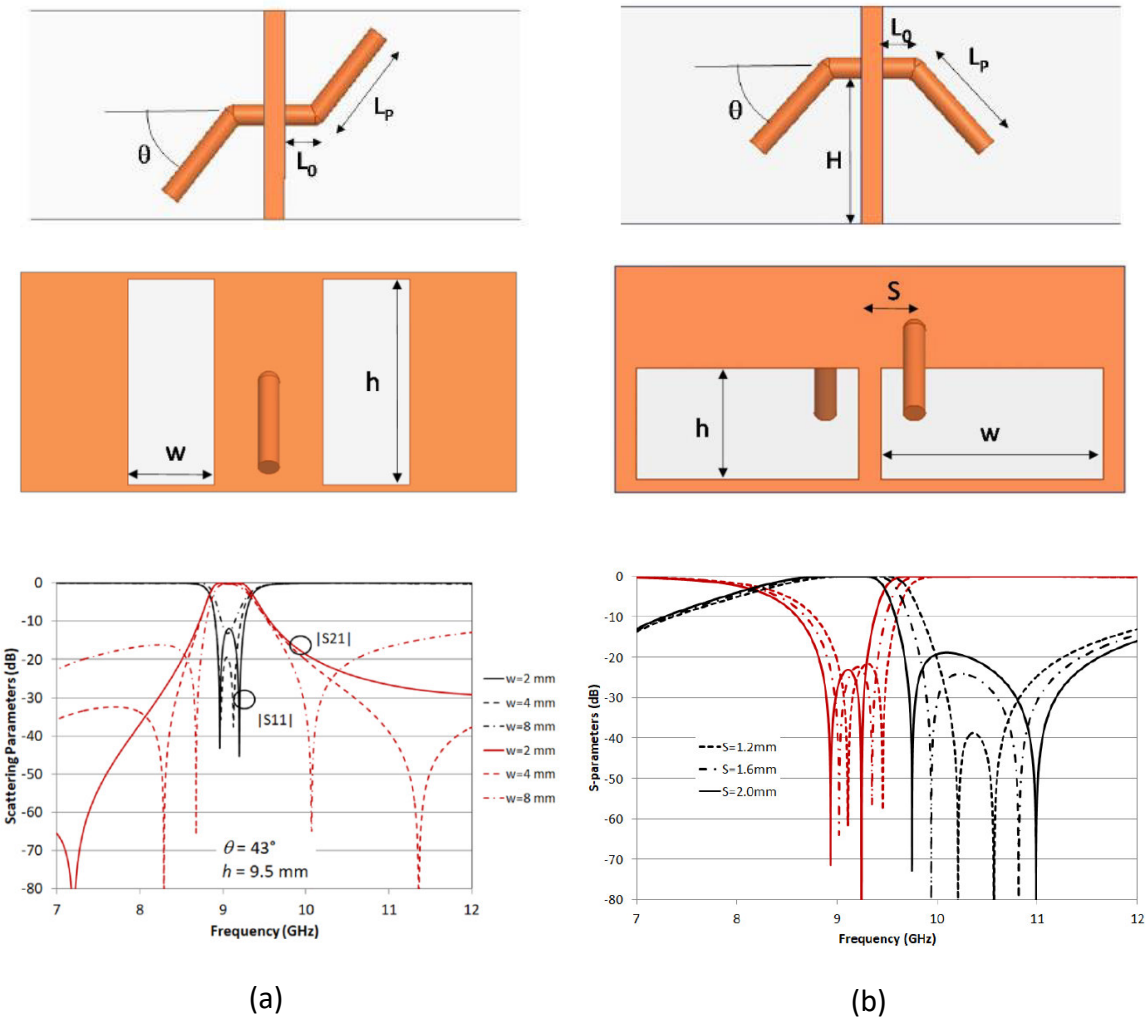

Figure P13. Very compact filtering structure composed of a single iris and two posts. The shape and size of the apertures and posts give the behavior of the filter [Tomassoni09]. (a) One transmission zero above and one below the pass-band of the filter (b) Two transmission zeros in the upper stop band

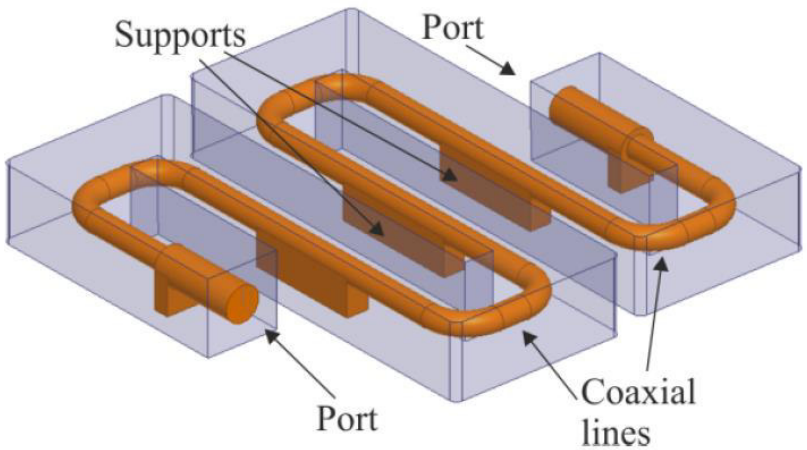

Figure P14. Inline coaxial filter where supports for the coaxial line behave as coupling elements [Venanzoni02].

Filter prototype	Measured over Reference *Q*-factor
Standard layout in aluminum	35 %
Shaped layout in aluminum	45 %
Shaped layout in aluminum with silver plating	157 %
Standard layout in titanium	14 %
Standard layout in titanium with chemical polishing	27 %
Shaped layout in titanium	18 %
Shaped layout in titanium with chemical polishing	33 %

Table B01. Comparison between measured and reference Q-factors of the filters manufactured through selective laser melting reported in [Lorente01].

Parameter	SLM	Micro-SLM
Laser power [W]	200	50
Beam spot diameter [μm]	100	30
Layer thickness [μm]	30	5
Powder particle size [μm]	20	5

Table B02. Typical values for some of the main parameters of the selective laser melting (SLM) and micro SLM processes.

Reference	Topology	Material	Center Frequency (GHz)	Fractional bandwidth (%)
Lorente01	5th-order filter with shaped waveguide cavities	AlSi10Mg, Titanium	11.0	1.8
Booth02	5th-order filter with shaped waveguide cavities and irises	Scalmalloy aluminum alloy	14.125	1.8
Booth03	9th-order filter with shaped waveguide cavities and irises	Scalmalloy aluminum alloy	12.875	1.9
Sattler01	4th-order filter with mushroom-shaped resonators	Stainless steel	7.924	3.9
Peverini02	5/6th-order filter with shaped stub resonators	AlSi10Mg, Ti6Al4V Stainless steel	13.75	18.2
Booth04	11th-order filter with shaped resonators	AlSi10Mg	18.75	15.5
Zhang01	15th-order H-plane waveguide filter with irises	CuSn15	73.5	6.9
Salek01	5th-order H-plane waveguide filter with irises	Stainless steel	90	11.1

Table B03. Comparison among filters developed with selective laser melting.

Reference	Filter Order/Geometry	3D technology	Center Frequency (GHz)	Fractional bandwidth (%)
[Montejio01]	4th-order filter / rect. waveguide inductive iris filter	FDM silverpainted	13,85	2.88
[Chappell04]	4th-order filter / stacked rectangular cavities	SLA electroplated	19.68	1.14
[Shang01]	5th-order filter / rectangular waveguide cavities	SLA copperplated	87.5	11.5
[Lucyszyn01]	4th-order filter / groove gap waveguide	PolyJet electroplated	35.65	1.4
[Shang04]	4th-order filter / helical resonators	SLA copper/silver plated	0.5	4
[Delhote02]	4th-order filter / reconfig. central freq.	FDM silverpainted	5.64	6.4
[Tomassoni08]	4th-order filter / mushroom-shaped resonators	SLA copperplated	0.81	6
[Venanzoni02].	4th-order filter / coaxial filter	SLA copperplated	3	1.6

Table P01. Comparison among filters developed through plastic AM.